JEM Journal of Experimental Medicine

ARTICLE

CtIP is essential for early B cell proliferation and development in mice

Xiangyu Liu[1,2*], Xiaobin S. Wang[1,3*], Brian J. Lee[1], Foon K. Wu-Baer[1], Xiaohui Lin[1], Zhengping Shao[1], Verna M. Estes[1], Jean Gautier[4], Richard Baer[1,4], and Shan Zha[1,4,5]

B cell development requires efficient proliferation and successful assembly and modifications of the immunoglobulin gene products. CtIP is an essential gene implicated in end resection and DNA repair. Here, we show that CtIP is essential for early B cell development but dispensable in naive B cells. CtIP loss is well tolerated in G1-arrested B cells and during V(D)J recombination, but in proliferating B cells, CtIP loss leads to a progressive cell death characterized by ATM hyperactivation, G2/M arrest, genomic instability, and 53BP1 nuclear body formation, indicating that the essential role of CtIP during proliferation underscores its stage-specific requirement in B cells. B cell proliferation requires phosphorylation of CtIP at T847 presumably by CDK, but not its interaction with CtBP or Rb or its nuclease activity. CtIP phosphorylation by ATM/ATR at T859 (T855 in mice) promotes end resection in G1-arrested cells but is dispensable for B cell development and class switch recombination, suggesting distinct roles for T859 and T847 phosphorylation in B cell development.

Introduction

The diversity and specificity of the adaptive immune system depend on the somatic assembly and subsequent modifications of the antigen receptor gene products. In particular, B lymphocyte development is achieved by multiple rounds of clonal expansion and two programmed DNA double-strand break (DSB) repair events at the Ig gene loci. V(D)J recombination assembles the exons that encode the variable region of the Ig genes in immature B cells, occurs exclusively in the G1 phase of the cell cycle, and is mediated exclusively by the nonhomologous end joining (NHEJ) pathway of DSB repair. Class switch recombination (CSR) modifies the constant region of the Ig heavy chain and results in different isotypes and thus effector function for the antibody, requires cell proliferation, and can be achieved by either NHEJ or the alternative end-joining (Alt-EJ) pathway that preferentially uses sequence microhomology (MH) to align the DSB junctions for repair. DNA resection, which converts DSB ends into 3′ single-stranded DNA (ssDNA) overhangs, promotes Alt-EJ by exposing flanking MH (McVey and Lee, 2008; Zhang and Jasin, 2011), and suppresses NHEJ by limiting KU binding (Mimitou and Symington, 2008; Symington and Gautier, 2011). Therefore, end resection is a critical determinant of the repair pathway choice in developing lymphocytes. In addition, end resection is also necessary for homologous recombination (HR), which is often necessary to support rapid cell proliferation.

C-terminal binding protein (CtBP)–interacting protein (CtIP) is best known as the mammalian orthologue of yeast Sae2, which initiates DNA end resection together with the MRE11–RAD50–NBS1 complex (Sartori et al., 2007; Mimitou and Symington, 2008; Cannavo and Cejka, 2014; Deshpande et al., 2016). In addition to DNA end resection, CtIP/Sae2 has also been implicated in nucleolytic processing of DNA hairpins (Lengsfeld et al., 2007; Makharashvili et al., 2014; Wang et al., 2014; Chen et al., 2015), removal of protein–DNA adducts (Nakamura et al., 2010; Aparicio et al., 2016; Deshpande et al., 2016), and termination of checkpoint signaling (Lengsfeld et al., 2007; Makharashvili et al., 2014; Wang et al., 2014; Chen et al., 2015).

CtIP protein contains several functional domains. Despite their primary sequence divergence, the N-terminal region of CtIP and Sae2 both mediate oligomerization necessary for end resection (Dubin et al., 2004; Wang et al., 2012; Andres et al., 2015). CtIP (897 amino acids in human) is much larger than Sae2 (345 amino acids). The middle of CtIP contains several motifs

[1]Institute for Cancer Genetics, Vagelos College of Physicians and Surgeons, Columbia University, New York, NY; [2]Guangdong Key Laboratory of Genome Instability and Human Disease Prevention, Shenzhen University Carson Cancer Center, Department of Biochemistry and Molecular Biology, School of Medicine, Shenzhen University, Shenzhen, China; [3]Pathobiology and Human Disease Graduate Program, Vagelos College of Physicians and Surgeons, Columbia University, New York, NY; [4]Department of Pathology and Cell Biology, Vagelos College of Physicians and Surgeons, Columbia University, New York, NY; [5]Division of Pediatric Oncology, Hematology and Stem Cell Transplantation, Department of Pediatrics, Vagelos College of Physicians & Surgeons, Columbia University, New York, NY.

*X. Liu and X.S. Wang contributed equally to this paper; Correspondence to Shan Zha: sz2296@cumc.columbia.edu; X. Liu's present address is Department of Biochemistry and Molecular Biology, Shenzhen University Medical Center, Shenzhen, China.

unique for CtIP, including those essential for its interaction with CtBP transcriptional repressor (through PLDLS motif; Schaeper et al., 1998), BRCA1 (S327) (Wong et al., 1998; Yu et al., 1998), and retinoblastoma-associated protein (Rb; E157; Liu and Lee, 2006) tumor suppressors, as well as its proposed intrinsic nuclease activities (Makharashvili et al., 2014; Wang et al., 2014). The C-terminus of CtIP shares the most homology with Sae2 (Sartori et al., 2007), including two conserved phosphorylation sites implicated in end resection. Specifically, CtIP is phosphorylated by cyclin-dependent kinase (CDK) and possibly the Polo-like kinases at T847 (S267 in Sae2) in S and G2 phases of the cell cycle (Chen et al., 2008; Huertas et al., 2008; Barton et al., 2014), and by ataxia telangiectasia and Rad3-related protein (ATR)/ataxia telangiectasia mutated (ATM) at T859 (S279 in Sae2) upon DNA damage (Peterson et al., 2013; Wang et al., 2013). Whether CtIP is essential for B cell development and how the specific domains/interaction partners of CtIP contribute to B lymphocyte development and Ig gene assembly and modification are not yet fully understood, in part due to the early embryonic lethality associated with the complete loss of CtIP (Chen et al., 2005). During V(D)J recombination, the hairpin coding ends (CEs) must be opened nucleolytically before end ligation, providing a unique opportunity to investigate whether mammalian CtIP can open hairpins outside the S/G2 phase.

Several attempts have been made to address the function of CtIP in B cells, especially during CSR. Knockdown of CtIP using shRNA in purified splenic B cells compromises CSR, which has been attributed to its direct contribution to Alt-EJ or its indirect effects on CDK2 activation or cell viability (Lee-Theilen et al., 2011; Buis et al., 2012; Polato et al., 2014). Knockin mouse models expressing S327A CtIP that cannot interact with BRCA1 are able to support both embryonic development (Reczek et al., 2013) and B cell CSR (Polato et al., 2014). In transgenic mouse models that express exogenous human CtIP proteins, embryogenesis and CSR can be rescued by expression of the phospho-mimetic CtIP-T847E mutant, but not the phospho-deficient CtIP-T847A mutant (Polato et al., 2014). In proliferating human cells, CtIP phosphorylation at T847 was proposed as a prerequisite for ATR/ATM–mediated hyperphosphorylation of CtIP upon DNA damage (Wang et al., 2013). However, in G1-arrested murine B cells, CtIP can still resect unrepaired DSBs in an ATM-dependent manner, but only in the absence of H2AX or 53BP1 (Helmink et al., 2011; Zha et al., 2011a; Liu et al., 2012; Oksenych et al., 2012), suggesting that CtIP can function outside S/G2, when CDK activity is minimal. However, it is unclear which CtIP residues, such as T859 (Peterson et al., 2013; Wang et al., 2013) or other potential ATM sites (Makharashvili et al., 2014), are relevant in G1. In *Xenopus* extract, phosphorylation of CtIP at T818 (corresponding to T859 in human CtIP) is essential for the recruitment of CtIP to the damaged chromatin (Peterson et al., 2013). In human cells, the expression of T859A mutant CtIP compromises end resection and HR (Wang et al., 2013), but the role of CtIP in early B cell development remains unknown, and how phosphorylation of CtIP at T859 contributes to lymphocyte development through the myriad functions of CtIP is also not known.

Using development stage–specific Cre recombinase and a conditional CtIP allele, we found that CtIP is essential for early B cell development, independent of V(D)J recombination, in part due to its ability to support continued proliferation at the G2/M transition. A genetic complementation screen reveals that the interaction of CtIP with CtBP, Rb, and Brca1 and its own nuclease activity are dispensable for B cell proliferation. Instead, the T847, but not the T859, phosphorylation of CtIP is essential for B cell development and switch recombination. Together these data indicate that in murine B cells, phosphorylation of CtIP at T859 has a cell cycle–independent role in end resection but is dispensable for B cell development in vivo.

Results

CtIP is essential for early B cell development but dispensable for the survival of peripheral naive B cells

To circumvent the embryonic lethality of *Ctip*-null mice, a conditional *Ctip* allele ($Ctip^{co}$) was inactivated specifically in precursor B cells using an Mb1/CD79a–driven Cre transgene ($Mb1^{Cre/+}Ctip^{co/co}$ mice) or in naive B cells using a CD21-driven Cre transgene ($CD21Cre^{+}Ctip^{co/co}$ mice; Kraus et al., 2004; Hobeika et al., 2006; Polato et al., 2014). Given B cell–specific deletion of CtIP, the relative frequency of B cells among all the hematologic lineages provides a measurement for B cell development in these mouse models. In contrast to CD19Cre (Rickert et al., 1997) used in prior studies, CD21Cre turns on only in IgM-positive naive B cells and achieves robust depletion of targeted protein in splenic B cells (Kraus et al., 2004). Consistent with prior studies (Lee-Theilen et al., 2011; Buis et al., 2012; Polato et al., 2014), CtIP depletion is well tolerated in naive mature B cells, as evidenced by the normal frequency and number of $B220^{+}IgM^{+}$ B cells in the bone marrow and spleen of $CD21Cre^{+}Ctip^{co/co}$ mice (Fig. 1 A and Table S1 A). However, upon activation, these *Ctip*-null B cells display severe proliferation defects and accumulate in the sub-G1 and G2 phases of the cell cycle (Fig. 1, B and C). Unlike V(D)J recombination, which is completed within the G1 phase, CSR requires cell proliferation (Franco et al., 2006). Thus, the severe proliferation defects of activated CtIP-deficient B cells likely contribute to the initial delay and moderate reduction of CSR (Fig. 1 B). Accordingly, CSR junctions recovered from activated $CD21Cre^{+}Ctip^{co/co}$ B cells are not significantly different from those of control $CD21Cre^{+}Ctip^{+/co}$ cells (Fig. 3 B). In contrast to naive B cells, the *Ctip*-null pre-B cells of $Mb1^{Cre/+}Ctip^{co/co}$ mice fail to thrive (Fig. 1 D), leading to severe reductions in the pre-, naive, and mature B cell frequency in the bone marrow and number and frequency in the spleen (Fig. 1, D and E; Fig. S1 A; and Table S1 A). There is also a notable reduction of pre-B/pro-B ratio in the bone marrow of $Mb1^{Cre/+}Ctip^{co/co}$ mice (Table S1 A). Although this observation is consistent with potential V(D)J recombination defects, the initiation of Cre expression in $Mb1^{Cre/+}$ mice also occurs at the pro-B to pre-B transition. A specific role of CtIP in V(D)J recombination was then tested in a cell-based system (see below). Meanwhile, T cell development and thymus cellularity

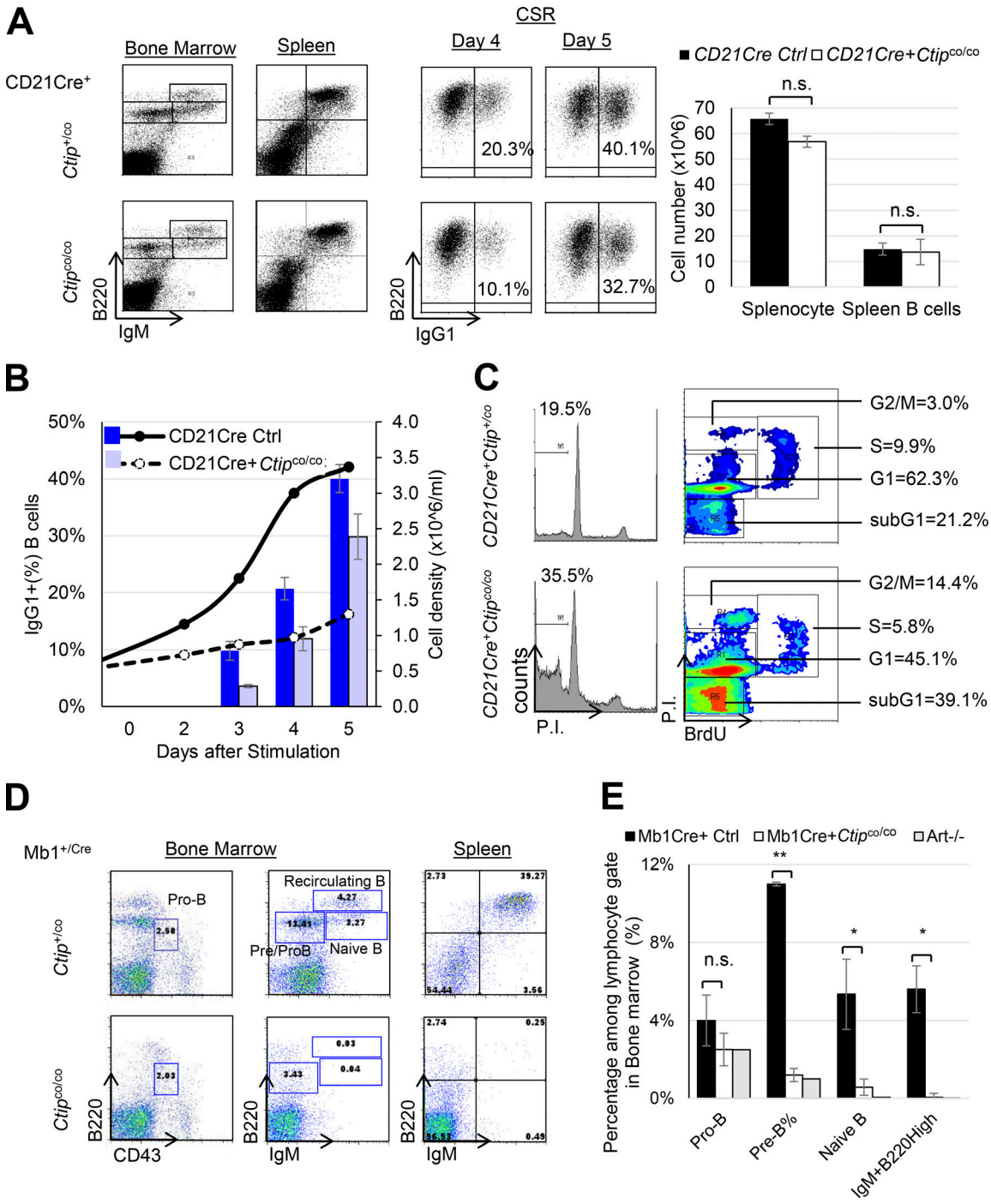

Figure 1. **CtIP is essential for immature B cells yet dispensable for naive B cells. (A)** Left: Representative flow cytometry analyses of lymphocytes in bone marrow and spleen from *CD21Cre*$^{+}$ *Ctip*$^{+/co}$ and *CD21Cre*$^{+}$ *Ctip*$^{co/co}$ mice. The boxes marked the IgM^{+}B220^{+} mature B cells. Middle: Representative flow cytometry analyses of purified CD43^{-} splenic B cells stimulated with LPS plus IL-4 for 4 and 5 d. The numbers indicate the percentage of IgG1^{+} B cells among all B cells (B220^{+}). The percentage of IgG1^{+} cells among all B220^{+} cells was marked on each blot. Right: Total splenocytes and B220^{+}IgM^{+} B cells in the spleens of *CD21Cre*$^{+}$ *Ctip*$^{+/co}$ and *CD21Cre*$^{+}$ *Ctip*$^{co/co}$ mice ($n \geq 4$ for each group). **(B)** Combo graph for CSR efficiency (percentage of IgG1^{+} cells, left y axis) and cell density (×10^{6}/ml, right y axis) from *CD21Cre*$^{+}$ *Ctip*$^{+/co}$ and *CD21Cre*$^{+}$ *Ctip*$^{co/co}$ mice ($n \geq 4$ for each group). **(C)** Representative cell cycle analyses of activated *CD21Cre*$^{+}$*Ctip*$^{+/co}$ and *CD21Cre*$^{+}$ *Ctip*$^{co/co}$ B cells pulse labeled with BrdU for 30 min before fixation and staining. Representative results from $n = 3$ biological repeats are shown. The boxes mark the sub-G1, G1, S (BrdU^{+}), and G2 populations. P.I., propidium iodide. **(D)** Representative flow cytometry analyses of lymphocytes from the bone marrow and spleens of *Mb1*$^{+/Cre}$ control and *Mb1*$^{+/Cre}$ *Ctip*$^{co/co}$ mice. Different B cell subtypes that were used to calculate the frequency and counts (Table S1 A) are marked in Fig. 1 D; they are pro-B cells (B220^{-}CD43^{+}), recirculating B cells (IgM^{+}B220^{high}), naive B cells (IgM^{+}B220^{+}) and pre/pro-B cells (IgM^{-}B220^{+}). **(E)** The frequency of B cell subtype in bone marrow. *Artemis*$^{-/-}$ (*Atr*$^{-/-}$) mice were used here as NHEJ-deficient control. Pro-B cells were defined as B220^{+}CD43^{+}. Pre-B cell frequency was calculated by substrating the frequency of pro-B cells from all IgM^{-} B cells in the bone marrow. Naive B cells are IgM^{+}B220$^{+(intermediate)}$ cells and the recirculated B cells are IgM^{+}B220^{high}. Two-tailed Student's *t* test was used to calculate P values ($n \geq 3$ for each group). The calculated absolute cell counts for each population were included in Table S1 A. Statistical significance was assessed using a two-tailed Student's *t* test (not significant [n.s.], P > 0.05; *, P < 0.05; **, P < 0.01). The error bars represent SD from three independent experiments.

are not affected in $Mb1^{Cre/+}Ctip^{co/co}$ mice (Fig. S1, B and C), supporting a cell-autonomous role for CtIP in pre-B cells (Table S1 A).

CtIP is dispensable for V(D)J recombination and NHEJ in G1 cells

Next, we examined whether the severe B cell developmental defects of $Mb1^{Cre/+}Ctip^{co/co}$, but not $CD21Cre^{+}Ctip^{co/co}$ mice reflect a role for CtIP in V(D)J recombination, including the opening of hairpin CEs (Fig. 1, B and C; Moshous et al., 2001; Rooney et al., 2002). Abelson murine leukemia virus–transformed pre-B cells (hereafter referred to as v-abl cells) containing an integrated V(D)J recombination reporter (pMX-INV) were derived from $Ctip^{co/co}$ mice, as described previously (Bredemeyer et al., 2006; Zha et al., 2011b). To induce CtIP inactivation, the $Ctip^{co/co}$ v-abl cells were infected with retrovirus-encoded WT CreER or recombinase-dead $CreER^{Mut(R173K)}$ (Jonkers et al., 2001). Induction of nuclear translocation of Cre with 4-hydroxytamoxifen (4OHT) effectively ablated the expression of WT *Ctip* in CreER-expressing cells, but not in $CreER^{Mut(R173K)}$-containing cells (Fig. 2 B). Induction of G1 arrest and the expression of recombination-activating gene (RAG) recombinase via the v-abl kinase inhibitor STI571 (imatinib) in CtIP-deleted cells leads to successful chromosomal V(D)J recombination at the integrated pMX-INV reporter (Fig. 2 A; as measured by the formation of both coding joins [CJs] and signal joins [SJs], as well as expression of GFP), regardless of CtIP depletion (Fig. 2, C and D). No measurable accumulation of unjoined CEs was detected in $Ctip^{-/-}$ cells (Fig. 2 D). Similar results were obtained in $Rosa26^{+/CreER\text{-}T2}Ctip^{co/co}$ v-abl cells, which harbor a knocked-in CreER-T2 allele in the *Rosa26* locus (Fig. S1 D). Sequence analyses of the SJs and CJs formed in the presence or absence of CtIP were also undistinguishable, with similar fidelity measured by ApaL1 digestion (Fig. 2 E) and a similar number of base-pair deletions and insertions (including both palindromic and non-template nucleotide addition; Fig. 2 F and Table S1 B). Moreover, ATM kinase inhibition similarly delays the joining phase of V(D)J recombination in both WT and *Ctip*-null cells without abolishing end joining or hairpin opening (Fig. S1 D). Artemis endonuclease is responsible for opening CE hairpins during V(D)J recombination (Moshous et al., 2001; Ma et al., 2002). In $Artemis^{-/-}$ cells, ectopic expression of the T847E human CtIP, but not the corresponding phospho-deficient mutant (T847A), leads to significant reduction of hairpin accumulation (Fig. 2 G), suggesting that phosphorylation of CtIP at T847 promotes CtIP-dependent hairpin opening. The low level of CtIP protein and the limited CDK activities in G1-arrested cells undergoing V(D)J recombination may explain why CtIP does not contribute to hairpin opening during physiological V(D)J recombination. Moreover, chromosomal breaks generated by the I-PpoI endonuclease is also efficiently repaired in $Ctip^{-/-}$ cells, in contrast to the lack of repair in $Xrcc4^{-/-}$ cells (Fig. S1 E). Taken together, these findings indicate that CtIP is dispensable for hairpin opening, general NHEJ, and RAG-mediated V(D)J recombination in murine B cells and that phosphorylation of CtIP at T847 promotes CtIP-mediated hairpin opening in lymphocytes.

CtIP deficiency leads to progressive loss of viability in proliferating lymphocytes mostly independent of ATR/ATM–mediated phosphorylation

While immature B cells are proliferative, naive B cells largely remain quiescent in the periphery. To test whether proliferation explains the apparent stage-specific requirements for CtIP in B cells, we compared the viability of G1 arrested versus proliferating B cells upon CtIP inactivation. Whereas CtIP inactivation is very well tolerated in STI571-treated, G1-arrested cells for ≥6 d, CtIP inactivation in proliferating cells led to a rapid loss of viability by day 3 or 4, as measured by the accumulation of small and rough cells with low forward scatter and high side scatter on flow cytometry analyses (Fig. 3, A and B). This loss of viability was delayed, but not prevented, by the expression of the EμBcl2 transgene (Fig. S2 D). Given the Tp53 pathway is routinely inactivated during v-abl–mediated transformation of immature B cells (Unnikrishnan et al., 1999), our findings suggest that loss of Tp53 function is also unable to prevent the lethality induced by CtIP inactivation.

To ascertain which domains/functions of CtIP are required to sustain lymphocyte proliferation, we performed genetic complementation experiments in $Rosa26^{+/CreER\text{-}T2}$ $Ctip^{co/co}$ cells by infecting them with retrovirus encoding WT or mutant human CtIP polypeptides followed by the internal ribosome entry site (IRES)–hCD2 surface marker (Figs. 3 C and S2 B). WT CtIP, but not the empty vector, rescued the viability of CtIP-deleted cells, leading to rapid accumulation (~10-fold enrichment) of $hCD2^{+}$ cells 6 d after the depletion of endogenous CtIP (+4OHT; Fig. 3 D). As expected, cell proliferation was also rescued by ectopic expression of the CDK phospho-mimicking mutant (CtIP-T847E), but not the phospho-defective mutant (CtIP-T847A; Fig. 3 D), consistent with the notion that CDK-dependent phosphorylation of CtIP at T847 is essential for viability (Polato et al., 2014). As shown in Figs. 3 D and S2 A, lymphocyte viability was also rescued by CtIP polypeptides bearing mutations that ablate its interaction with CtBP (CtIP-ΔPLDLS; Schaeper et al., 1998) or Rb (CtIP-E157K; Fusco et al., 1998) or abrogate its intrinsic MRE11–RAD50–NBS1–independent nuclease activity (e.g., N181A/R185A, E267A/E268A, and N289A/H290A; Makharashvili et al., 2014; Wang et al., 2014). Finally, the viability of the proliferating cells was fully restored by CtIP-T859E and only partially rescued by CtIP-T859A (Fig. 3 D). Similar partial restoration of cell proliferation was also observed upon ectopic expression of a CtIP mutant (S231A/S664A/S745A) that lacks three other proposed ATR/ATM phosphorylation sites outside the conserved C-terminal domain (Fig. 3, B and C). Together, these findings suggest that ablation of the ATR/ATM–mediated phosphorylation of CtIP might provide an opportunity to separate the end-resection role of CtIP from its essential role in cell proliferation.

Phosphorylation of CtIP at T859 is important for end resection in G1-arrested cells

To determine whether T859 phosphorylation of CtIP can promote end-resection in G1 cells independent of CDK dependent phosphorylation, we generated $Rosa26^{+/CreER\text{-}T2}Xrcc4^{-/-}53BP1^{-/-}Ctip^{co/co}$ cells in which the unrepaired (due to XRCC4 deficiency)

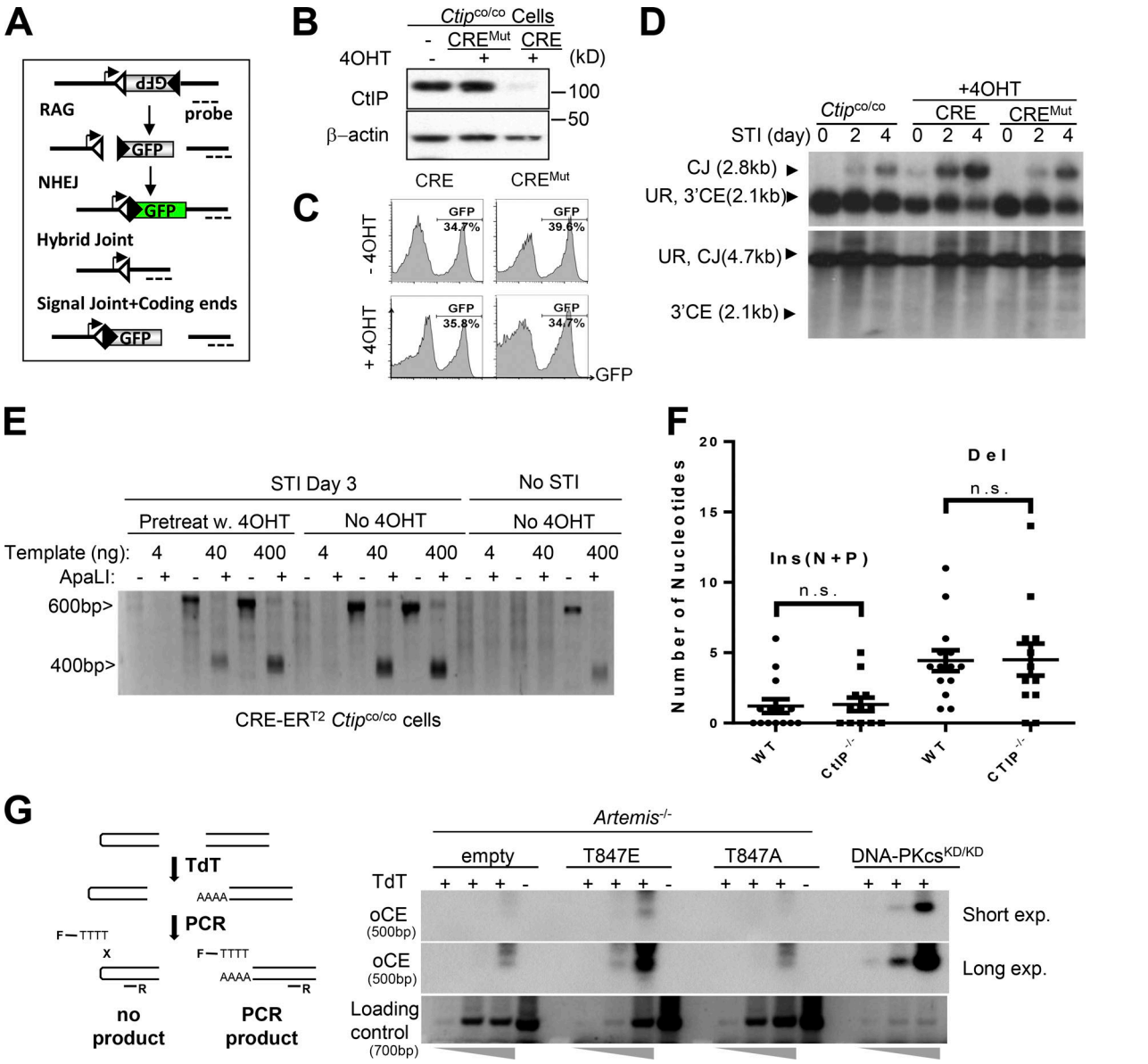

Figure 2. **CtIP is not required for NHEJ and chromosomal V(D)J recombination. (A)** Schematic of pMX-INV V(D)J recombination substrates. The unrearranged substrate, hybrid join, coding/signal end intermediates, and CJs/SJs are diagrammed. The recombination signal sequence (triangle) and hCD4 probe (dashed lines) are indicated. **(B)** Western blot for CtIP and actin on Ctip$^{co/co}$ cells carrying ER-Cre (WT or mutant) treated with 4OHT (0.2 µM). **(C and D)** FACS (C) and Southern blot analyses (D) of pMX-INV rearrangement products (expressed GFP) in ER-Cre^{+} *Ctip*$^{co/co}$ cells treated with 4OHT. The percentage of GFP^{+} cells are marked on the histograms. UR, unrearranged. **(E)** Semiquantitative PCR analyses (10-fold dilution) of the SJs formed in *Rosa*$^{ERCreT2/+}$*Ctip*$^{co/co}$ cells treated with STI571 (STI) with or without pretreat with 4OHT (for 24 h) to inactivate CtIP. Precise SJs formed in the pMX-INV substrate can be digested by ApaL1. **(F)** Comparison of the number of nucleotide deletion (Del) and insertion (Ins; including both nontemplate and palindromic elements) in de novo CJs formed in *Ctip*$^{Co//Co}$ (WT) and *Ctip*$^{-/-}$ cells. Each dot represents a unique CJ (n = 14 for WT and n = 12 for *Ctip*$^{-/-}$ cells). The junction sequences are presented in Table S1 B (P = 0.8655 for insertion and P = 0.9576 for deletion). **(G)** Diagram (left) and results (right) of the TdT-mediated ligation PCR assay. If the hairpin is opened, then TdT adds a poly(A) tail to the ends, which can be subsequently amplified via PCR using universal primer complementary to the poly(A) tail. The PCR product (~500 bp) was detected with p32-labeled oligo probes against hCD4. PCR corresponding to the Rosa26 locus was used as loading control. Two biological repeats support the same conclusion. One representative result is shown. Statistical significance was assessed using a two-tailed Student's t tests (n.s., not significant). F, forward; N, nontemplated nucleotide addition; P, palindromic nucleotide addition; R, reverse. The error bars represent SD from three independent experiments.

RAG-generated DSBs in G1-arrested (STI571-treated) cells are rapidly degraded in the absence of 53BP1 or H2AX (Fig. 3 E, lane 2; Helmink et al., 2011; Zha et al., 2011a; Liu et al., 2012; Oksenych et al., 2012). In these cells, inactivation of CtIP (via +4OHT) completely prevented end degradation and restored normal levels of unrepaired CEs (lane 4), providing a system to measure CtIP-dependent end resection in G1, presumably independent of CDK phosphorylation. Moreover, ATM inhibition partially inhibits CE degradation in *Ctip*$^{+/+}$ cells (lane 3) without affecting CE levels in *Ctip*$^{-/-}$ cells (lane 5), supporting an epistatic relationship between

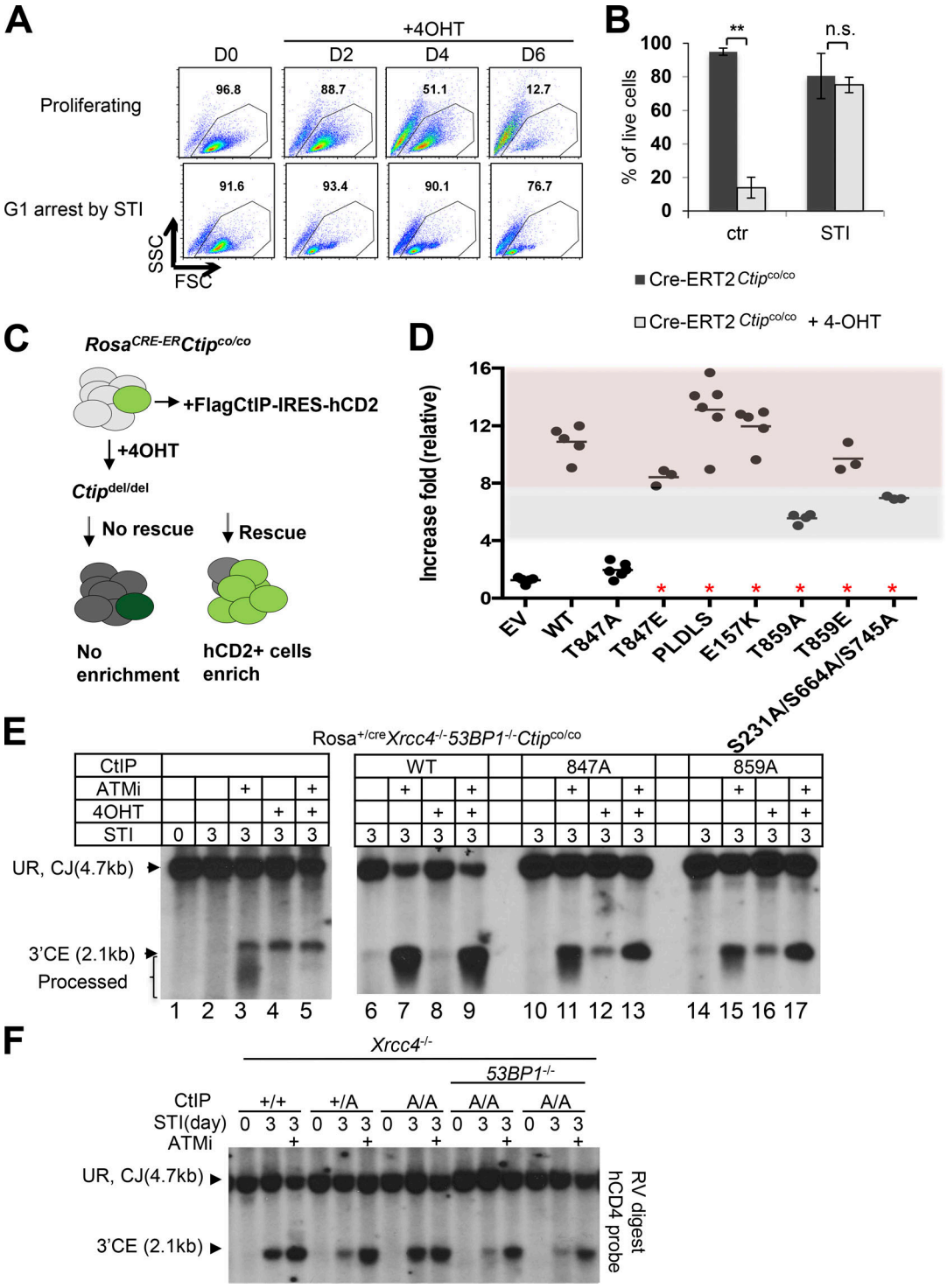

Figure 3. **CtIP is essential for continued proliferation of B cells. (A)** Representative FACS analyses of *Rosa26*$^{+/CreER\text{-}T2}$Ctip$^{co/co}$ cells treated with 4OHT and with/without cocurrent treatment with STI571 (STI; 3 µM). FSC, forward scatter; SSC, side scatter. **(B)** The percentage of live cells after 4OHT treatment was determined by forward and side scatter. The data represent the average and SD of three or more independent experiments collected at day 6 after 4OHT treatment. **(C)** Diagram for the CtIP rescue experiment. Retrovirus encoding Flag-tagged human CtIP-IRES-hCD2 was used to infect *Rosa26*$^{+/CreER\text{-}T2}$*Ctip*$^{co/co}$ cells. The fold of enrichment for hCD2^{+} cells after 4OHT treatment (deletion of endogenous CtIP; for 6–9 d) compared with before 4OHT treatment was plotted. Cells with the expression of WT-CtIP or mutants that support cell viability accumulate after the deletion of endogenous CtIP, leading to ∼10-fold enrichment for the percentage of hCD2^{+} cells in the culture (e.g., from 2.5% to nearly 25% among the live cells). **(D)** Statistical analyses of the rescue experiments for indicated CtIP mutants. The rescue experiments were repeated four to six times for each CtIP mutant. EV, empty vector. **(E)** Southern blot analyses of CEs of pMX-INV substrate in *Rosa26*$^{+/CreER\text{-}T2}$ *XRCC4*$^{-/-}$*53BP1*$^{-/-}$*Ctip*$^{co/co}$ cells mock infected (lanes 1–5) or infected with retrovirus encoding either WT human CtIP (lanes 6–9) or the indicated CtIP mutants (lanes 10–17). Individual cultures were then treated with or without ATM inhibitor (ATMi), 4OHT, and/or STI571, as indicated. **(F)** pMX-INV substrate analyses in *Xrcc4*$^{-/-}$*53BP1*$^{-/-}$*Ctip*$^{T855A/T855A}$ cells and controls. Statistical significance was assessed using a two-tailed Student's *t* test (n.s., P > 0.05; **, P < 0.01). RV, EcoRV; UR, unrearranged.

ATM and CtIP with respect to end resection in these cells. Complete degradation of CEs in the *Ctip*$^{-/-}$ cells (+4OHT) was restored by the expression of WT human CtIP (lane 8), but not the CtIP-T847A (lane 12) or CtIP-T859A mutants (lane 16). ATM inhibition further promoted CEs accumulation in CtIP-T847A– or CtIP-T859A–expressing cells (lanes 13 and 17), consistent with the existence of other ATM phosphorylation sites on CtIP. B cell lines derived from mouse carrying the knockin mutation corresponding to T859A (T855A in mouse) in the germline (*Ctip*$^{T855A/T855A}$) also show reduced end resection (see below; Fig. 3 F). Together, these observations suggest that phosphorylation of CtIP at T859 (T855 in mouse) promotes end resection in G1 phase cells together with other ATR/ATM phosphorylation sites.

Normal lymphocyte development in *Ctip*$^{T855A/T855A}$ mice

Consistent with the ability of exogenous human CtIP-T859A to partially support lymphocyte proliferation in culture (Fig. 3 D), mice with an alanine substitution at the corresponding T855 residue (*Ctip*$^{T855A/T855A}$) are of normal size (Fig. S3 A) and normal thymus and spleen cellularity (Fig. S3 D) and have normal development of B cells and T cells (Fig. 4 A; Fig. S3, B and C; and Table S1 A). A minor yet consistent reduction in the frequency of CD3^{high}CD4^{+}CD8^{+} immature thymocytes was noted in *Ctip*$^{T855A/T855A}$ mice (Fig. 4 A). In previous studies, similar reductions of surface CD3 levels in thymocytes from ATM- or 53BP1-deficient mice have been attributed to defects in maturation from double-positive to single-positive T cells (Borghesani et al., 2000; Difilippantonio et al., 2008). Sequence analyses of the V(D)J recombination junctions in both B cells (IgH) and T cells (TCRβ) did not find any significant difference in SJ fidelity or CJ palindromic and nontemplate nucleotide addition or deletion (Fig. S3 E; and Table S1, C and D). Moreover, despite a moderate and transient delay at day 3, *Ctip*$^{T855A/T855A}$ B cells undergo robust CSR upon activation in vitro (Figs. 4 B and S3 F). Consistent with the partial rescue in the reconstitution experiments (Fig. 3 D), activated *Ctip*$^{T855A/T855A}$ B cells show a moderate reduction in overall proliferation (Fig. 4 C). However, the frequency of IgG1^{+} B % cells does not significantly differ in *Ctip*$^{T855A/T855A}$ B cells versus the control (P = 0.74) at each cell division, suggesting T855A-CtIP does not directly compromise IgG1 switching beyond cell proliferation. Moreover, high-throughput sequencing analyses of >10,000 CSR junctions between Sμ and downstream switch regions show that the usage of peripheral switch regions (an indicator of end resection) and the number of MHs at the junction (an indicator of Alt-EJ) are also not affected by the T855A mutation of CtIP (Fig. 4, D and E). Taken together, these findings indicate that ATR/ATM–mediated phosphorylation of CtIP at T859 promotes end resection but is largely dispensable for CSR, V(D)J recombination, and lymphocyte viability in vivo.

CtIP-deficient cells accumulate at the G2/M checkpoint

We next investigated how *Ctip* inactivation compromises the viability of proliferating immature B cells. The loxP recombination signals of the conditional *Ctip*^{co} allele flank exon 2, which encodes the initiator methionine codon and most of the CtIP tetramerization domain (Bothmer et al., 2013). In v-abl–transformed *Rosa26*$^{+/CreER\text{-}T2}$*Ctip*$^{co/co}$ cells, 4OHT leads to complete absence of full-length CtIP protein by 24 h and expression of a truncated CtIP protein lacking the N-terminal tetramerization domain (Fig. S4 A). Consistent with the essential role of oligomerization in CtIP function (Davies et al., 2015; Forment et al., 2015), this truncated CtIP polypeptide does not support embryonic development (Bothmer et al., 2013), immature B cell development (Fig. 1 C), or the viability of proliferating immature B cell in culture (Fig. 3 A).

Within 24 h of Cre induction, *Rosa26*$^{+/CreER\text{-}T2}$*Ctip*$^{co/co}$ cells displayed a marked increase in phosphorylation of the ATM substrates KAP1 and CHK2, as well as a decrease in mitosis-specific phosphorylation events (e.g., pH3Ser10 and pCdc2; Fig. 5 A and Fig. S4, A and B). Cell cycle analyses revealed progressive loss of BrdU^{+} S phase cells (from 62.5% to 2.3%), prominent G2/M accumulation (BrdU^{-}, 4N cells; from 5.8% to 39.6%; Fig. 5 B), and decreased mitotic cell (pH3Ser10^{+}) frequency in the G2/M pool (Fig. 5 C), all of which are consistent with G2/M cell cycle arrest. Phosphorylation of CHK1 at S345, a substrate of ATR kinase, increases transiently 2 d after *Ctip* inactivation (Fig. 5 A), while total CHK1 protein levels are reduced by day 3, consistent with phosphorylation-dependent ubiquitination and degradation of CHK1 during persistent G2/M arrest (Zhang et al., 2005, 2009). Meanwhile, CtIP-deleted cells arrested in G1 (by either CDK4/6 inhibitor or STI571) can enter S phase and initiate DNA synthesis upon release, despite a moderate delay (Fig. S4, F and G), suggesting that CtIP is not essential for the initiation of S phase of DNA replication. CtIP-deleted cells also harbor high levels of 53BP1 nuclear bodies, which typically arise from aberrant processing of underreplicated DNA during the previous mitosis (Lukas et al., 2011; Fig. 5 D). As observed for CtIP-deficient splenic B cells (Polato et al., 2014), cytogenetic analysis of immature B cells harvested 24 h after CtIP inactivation showed increased levels of chromosome and chromatid breaks (Figs. 5 E and S4 E), as well as frequent accumulation of micronuclei (Fig. 5 F).

In mammalian cells, the G2/M cell cycle checkpoint is induced in response to DNA damage by ATM kinase (Beamish et al., 1994; Xu et al., 2002). Interestingly, the Sae2 protein in yeast acts to attenuate checkpoint signaling by limiting Tel1 activation (the yeast ATM orthologue; Chen et al., 2015). As a consequence, Sae2-deficient cells exhibit reduced survival due to persistent checkpoint signaling and cell cycle arrest. To ascertain if a similar mechanism contributes to the reduced viability of *Ctip*-deleted lymphocytes, we tested whether inhibition of ATM signaling would delay cell death upon CtIP loss. In contrast to yeast, in B lymphocytes, ATM inhibition and ATM deletion failed to restore the viability of *Ctip*-deleted cells (Figs. 5 G and S4 D). Instead, ATM inhibition greatly increased the frequency of nuclear fragmentation in *Ctip*-deleted cells (Fig. 5 F), suggesting that the ATM-mediated G2/M checkpoint protects CtIP-deficient cells from mitotic DNA fragmentation. Together, these findings suggest that CtIP inactivation leads to an accumulation of aberrant recombination/replication intermediates, which activate ATM and induce G2/M cell cycle arrest.

Ku70 deletion enhances G2/M arrest and delays cell death associated with CtIP deficiency

Next, we tested whether partial restoration of DNA end resection via KU deletion or EXO1 activation can restore the viability

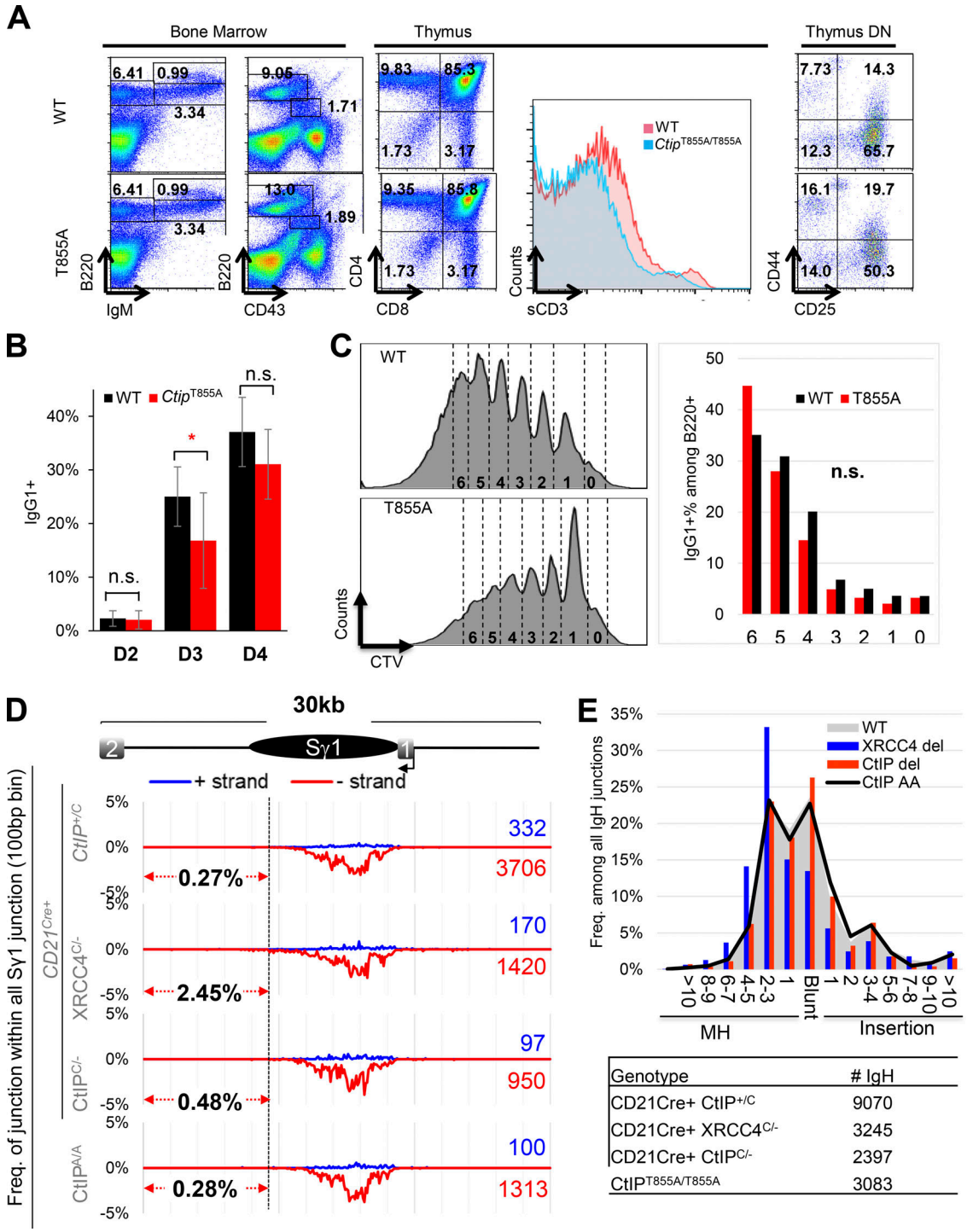

Figure 4. **T859 phosphorylation of CtIP is dispensable for normal B cell development and CSR. (A)** Representative flow cytometry analyses of lymphocyte development of 7–8-wk-old *Ctip*$^{+/+}$ and *Ctip*$^{T855A/T855A}$ mice ($n \geq 3$ mice of each genotype). The boxes on the B220-IgM plots represent IgM$^-$B220$^+$ pre- or pro-B cells, IgM$^+$B220^{high} recirculating B cells, and IgM$^+$B220$^+$ naive B cells, respectively. The boxes on the B220$^-$CD43 plots represent B220$^+$CD43$^+$ pro-B cells. The percentage of each gated population is marked on the dot plots. DN, CD4$^-$ and CD8$^-$ double negative T cells. **(B)** Statistical analyses of IL-4 plus LPS-stimulated B cells (CD43$^-$ splenocytes) from *Ctip*$^{+/+}$ and *Ctip*$^{T855A/T855A}$ mice ($n \geq$ mice of each genotype). The bar graphs represent the average and SE (P = 0.064 at day 2, 0.023 at day 3, and 0.11 at day 4). **(C)** The CTV labeling for cell proliferation in activated splenic B cells from *Ctip*$^{+/+}$ and *Ctip*$^{T855A/T855A}$ mice. The switch percentage in each respective cell division is plotted on the right (P = 0.74 via Student's *t* test). **(D)** The spatial distribution of prey-break sites in Sγ1 presented as the frequency (%) of Sγ1 prey-break sites that falls into each 100-bp bin. The pool of all data from each genotype was plotted. All (–, red, from telomere to centromere orientation) and (+, blue, from centromere to telomere orientation) strand prey breaks add up to 100%. For each genotype, the number of total (+) strand (blue) and (–) strand (red) junctions are marked on the right. The dashed lines indicate the percentage of (–) strand Sγ1 prey that fall outside the core Sγ1 region. **(E)** The distribution of IgH junctions by junctional sequence features (blunt). This panel represents the pool of IgH junctions from each genotype. The numbers of junctions from each genotype are listed in the small table in the figure ($n >$ 2,300 for each genotype). Statistical significance was assessed using a two-tailed Student's *t* test (n.s., P > 0.05; *, P < 0.05).

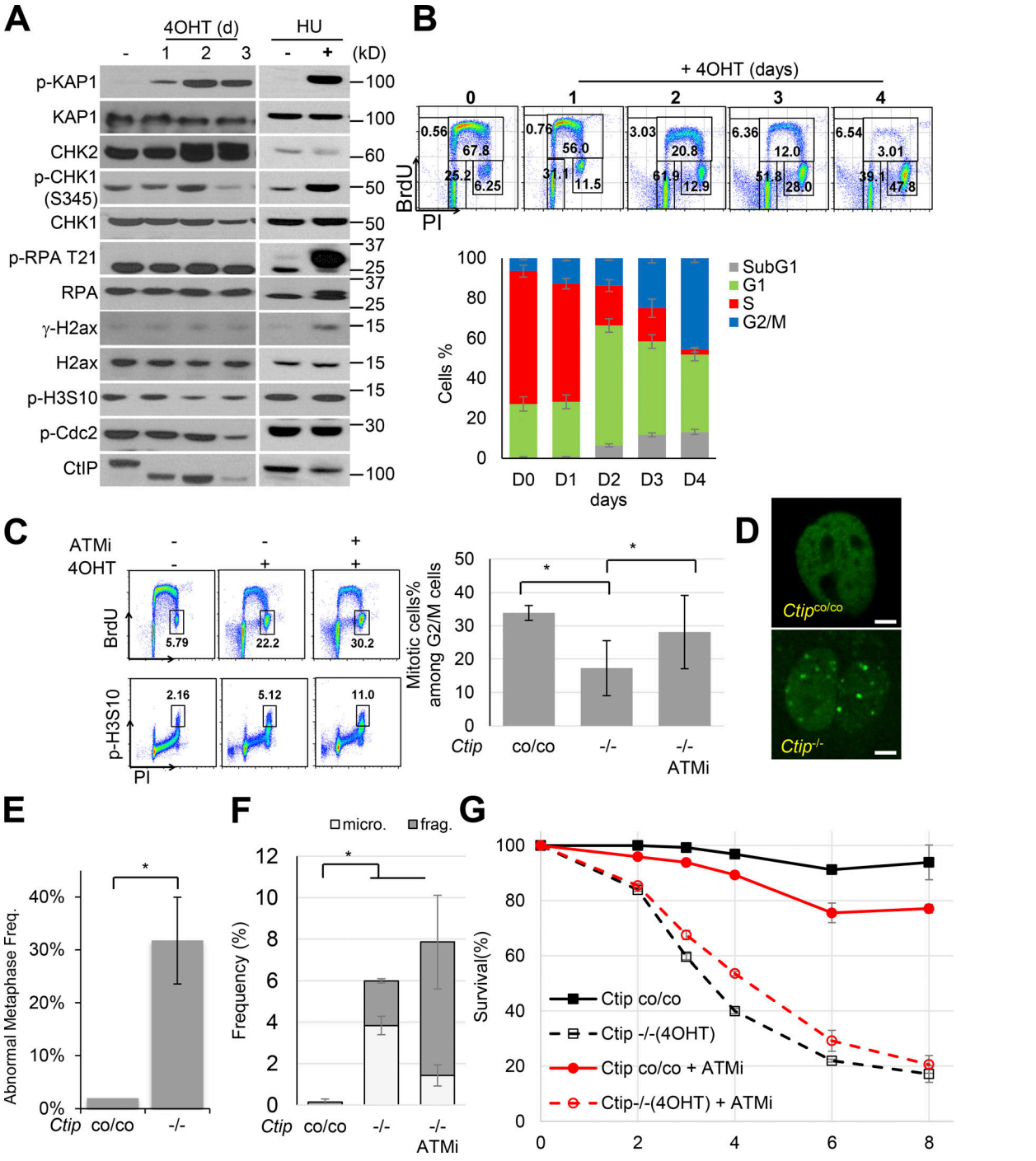

Figure 5. **Hyperactivation of ATM and G2/M cell cycle arrest upon *Ctip* inactivation in B cells. (A)** Western blotting analyses of Abelson cells upon *Ctip* inactivation via 4OHT (days 1–3). HU-treated $Ctip^{co/co}$ cells are shown as positive control. **(B)** Representative cell cycle analyses and quantification of cell cycle changes upon Cre activation in $Rosa26^{+/CreER\text{-}T2}Ctip^{co/co}$ B cells. The boxes represent the G1, S, and G2 populations. The data represent the average and SD of $n \geq 3$ biological repeats. PI, propidium iodide. **(C)** Representative flow cytometry analyses and quantification of pHistone3-Ser10–positive cells among $BrdU^{-}$G2/M cells. Experiments were repeated three times on two independently derived lines. The boxes mark the G2 (upper) and mitotic (lower, $pH3Ser10^{+}$) cells. **(D)** Representative images show the 53BP1 nuclear body in $Ctip^{-/-}$ cells. Representative images from two independent experiments and $n \geq 6$ cells acquired were shown. Scale bars, 5 µm. **(E)** Quantification of metaphases with abnormalities (including chromosomal and chromatid breaks) in $Rosa26^{+/CreER\text{-}T2}$ $Ctip^{co/co}$ B cells with ($Ctip^{-/-}$) or without ($Ctip^{co/co}$) Cre activation. The data represent the average and SD of $n \geq 3$ biological repeats. **(F)** The frequency of the cells with micronuclei or fragmented nucleus in WT and Ctip-deficient Abelson cells. The data represent the average and SD of $n \geq 3$ biological repeats. **(G)** Representative cell viability analyses for $Rosa26^{+/CreER\text{-}T2}Ctip^{co/co}$ cells treated with ATM inhibitor (ATMi) or 4OHT to active Cre recombination. The data represent the average and SD of $n \geq 3$ biological repeats. Statistical significance was assessed using a two-tailed Student's *t* test (*, $P < 0.05$).

of CtIP–deficient cells (Mimitou and Symington, 2010; Symington and Gautier, 2011). Although KU deletion does not rescue the embryonic development of CtIP-deficient mice (Polato et al., 2014), we observed a significant delay in cell death upon codeletion of Ku in *Rosa26*$^{+/CreER\text{-}T2}$*Ku70*$^{-/-}$*Ctip*$^{co/co}$ v-abl cells (Fig. 6 A). This delay is not due to the lack of DNA-dependent protein kinase (DNA-PK) activity, since DNA-PK kinase inhibitor does not delay cell death upon CtIP inactivation (Fig. S3 G). Ku deletion in CtIP-deficient cells elicits hyperphosphorylation of the ATM substrates KAP1 and CHK2 (Fig. 6 B), enhances G2/M arrest, and delays the loss of S phase and BrdU$^+$ populations. ATR kinase inhibition also delays cell death in CtIP-deleted cells and appears to act epistatically to CtIP deletion (Fig. 6 D), suggesting that defects in end resection potentially suppress basal ATR activity (as measured by CHK1 phosphorylation) during normal cell proliferation to affect the viability of CtIP-deleted cells. Using ATM- or ATR-specific inhibitors, we confirmed that in CtIP-deficient cells, ATM is responsible for hyperphosphorylation of KAP1 and CHK2, while ATR is responsible for CHK1 phosphorylation (S345; Fig. 6 E). Notably the level of γH2AX and pRPA(T21) also increased in KU70-deficient cells, consistent with the requirement for KU70 in NHEJ and in preventing end resection, which likely enhance ATM and ATR activation and G2/M arrest. Together, these findings suggest that CtIP-mediated end resection might be necessary to process certain types of replication intermediates to generate ssDNA and basal ATR signaling during replication.

CtIP contributes to the processing of Top1cc-like lesions

To identify the features of lesions that trigger ATM activation and G2/M arrest in CtIP-deleted cells, we challenged *Ctip*$^{-/-}$ B cells with several genotoxins with defined mechanisms of action. WT and CtIP-deleted cells were treated with ionizing radiation (IR; Fig. S3 H), hydroxyurea (HU; Fig. 7 A), or the topoisomerase I inhibitor camptothecin (CPT; Fig. 7 B) at 24 h after Cre activation, a time point at which CtIP is deleted, the cell cycle distribution of *Ctip*$^{-/-}$ cells is not significantly altered (Figs. 5 B and 6 C), and there is no significant DNA DSBs detected via neutral comet assay (Fig. S4 C). CtIP inactivation did not affect HU-induced CHK1 phosphorylation (Fig. 7 A) or IR-induced phosphorylation of KAP1 and CHK2 (Fig. S3 H), suggesting that CtIP does not directly affect ssDNA-induced ATR activation or DSB-induced ATM activation. In contrast, CtIP deficiency markedly attenuates CPT-induced RPA (replication protein A) and CHK1 phosphorylation while enhancing KAP1 and CHK2 phosphorylation in a dose-dependent manner (Fig. 7 B), similar to what was found in *Ctip*$^{-/-}$ proliferating B cells at later time points (Fig. 3 E). *Ku70* deletion partially restores RPA and CHK1 phosphorylation and intensifies KAP1 and CHK2 phosphorylation in CPT-treated CtIP-deficient cells, consistent with the notion that the end-resection defect of these cells is ameliorated by the loss of *Ku70* (Fig. 7 D). *Ctip*$^{T855A/T855A}$ B cells do not show spontaneous hyperphosphorylation of KAP1/CHK2 or reduced CHK1/RPA phosphorylation under these conditions. Although CPT-induced pRPA and pCHK1 occurs reproducibly in *Ctip*$^{T855A/T855A}$ cells and much higher than those in *Ctip*$^{-/-}$ cells, there are moderate reductions in comparison to *Ctip*$^{+/+}$ B cells (Fig. 7 E). Meanwhile, IR- and CPT-induced chromatin accumulation of CtIP is also moderately reduced in *Ctip*$^{T855A/T855A}$ B cells (Fig. 7 F), consistent with the previous finding in *Xenopus* extracts (Peterson et al., 2012). Taken together, our findings suggest that CtIP normally processes replication/recombination intermediates (e.g., Top1cc-like lesions) during S/G2 phase in a T847 phosphorylation–dependent but largely T859 phosphorylation–independent manner. In the absence of CtIP, the failure to process these replication intermediates contributes to loss of cellular viability, in part through hyperactivation of ATM and prolonged G2/M arrest and premature entry into mitosis with unrepaired and/or underreplicated DNA.

Discussion

Although the role of CtIP in DNA end resection has been extensively studied at the biochemical level, the in vivo functions of CtIP in lymphocyte development are less clear owing to its requirement for embryonic development. Using a conditional allele, we found that CtIP is dispensable in peripheral naive B cells but essential for early B cell development. We further showed that this requirement for CtIP in early B cells is independent of its role in V(D)J recombination, reflecting its critical role in continuous proliferation. Using G1-arrested B cells, we found that ectopic expression of T847E CtIP, but not endogenous CtIP or T847A CtIP, is able to open CEs hairpins. These data suggest that hairpin opening might be regulated in a cell cycle–dependent manner, mediated exclusively by Artemis during G1 and by Artemis and/or CtIP in S and G2 cells.

CtIP binds both CtBP and Rb. While tissue-specific interactions in other cell lineages cannot be excluded, the essential role of CtIP in B cell proliferation does not require its readily detected interaction with CtBP or Rb. While phosphorylation of CtIP at T847 (likely by CDK) is required both for CtIP-mediated DNA resection of unrepaired DSBs and for the viability of proliferating lymphocytes, phosphorylation of CtIP at T859 (presumably by ATR/ATM) is important for CtIP-mediated resection in G1-arrested cells (Fig. 3 E) and cycling cells (Fig. 7 E; Peterson et al., 2013) but is not essential for proliferating lymphocytes. It is possible that CtIP is essential for the nucleolytic processing of complex DNA substrates beyond simple DSBs. In this context, we found that T847 phosphorylation is uniquely required for hairpin opening. Activation of ATM in *Artemis*$^{-/-}$ cells is not sufficient to activate the hairpin-opening activity of CtIP (Fig. 2 F). Other studies have highlighted an important role of CtIP in complex genomic structures (Makharashvili et al., 2014; Wang et al., 2014), including the CPT lesion we verified in murine lymphocytes here (Fig. 7 E). In this case, CtIP does not seem to play a role in the resection of IR-generated breaks (at least not at the early time points measured here). In addition, the amount of resection in G1 might be much lower than what was needed in S/G2 and during proliferation. This hypothesis is supported by the dramatic increase of CtIP protein levels in S/G2 phase cells (Yu et al., 1998), in addition to the CDK-mediated phosphorylation at T847. Thus, T859 phosphorylation, while dispensable for lymphocyte development and CSR, provides a mean to fine-tune CtIP activity upon DNA damage in S/G2 phase.

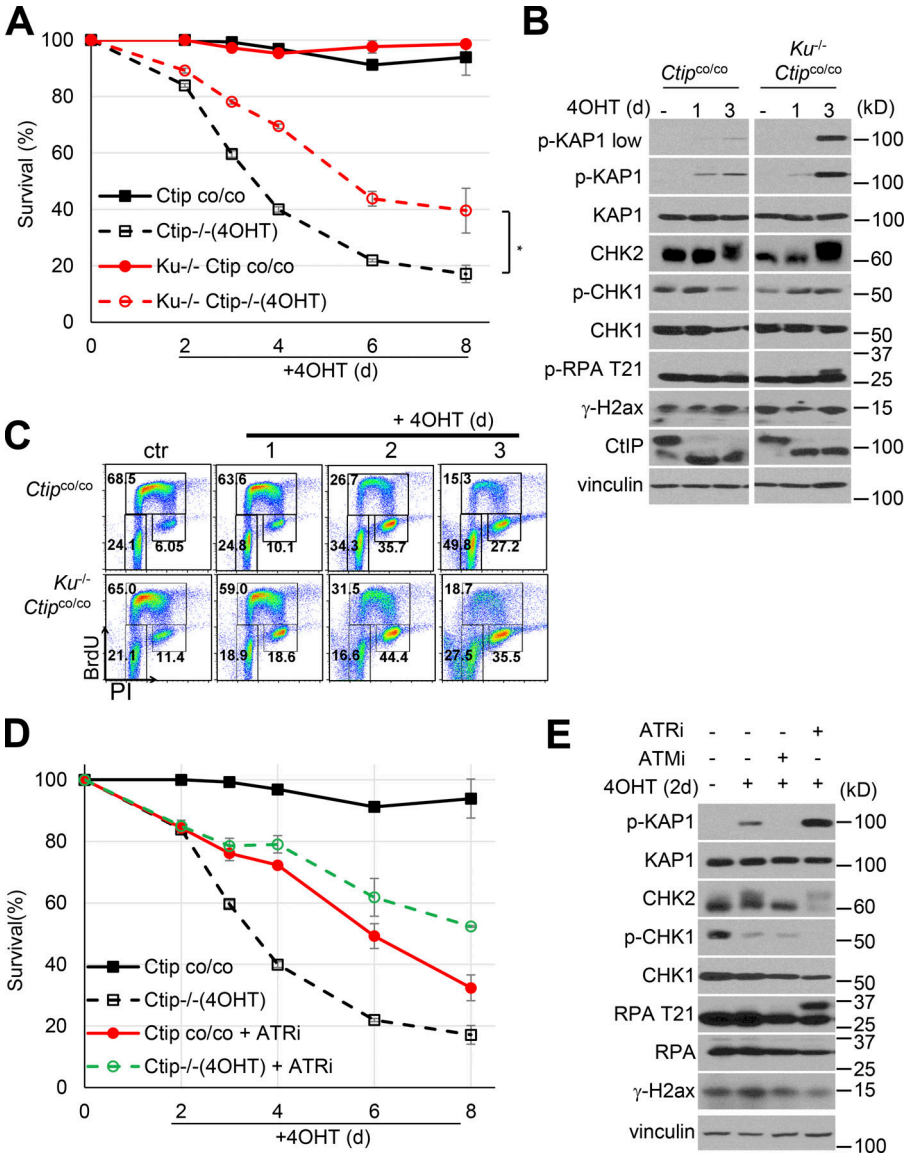

Figure 6. **Ku deletion and ATR inhibition delay cell death upon *Ctip* inactivation. (A)** Representative cell viability analyses for *Rosa26*$^{+/CreER\text{-}T2}$*Ctip*$^{co/co}$ and *Rosa26*$^{+/CreER\text{-}T2}$*Ctip*$^{co/co}$*Ku70*$^{-/-}$ cells treated with 4OHT. The data represent the average and SD of $n \geq 3$ biological repeats. Ku70 deficiency significantly ($P < 0.01$) rescued the viability of CtIP-deficient cells at all time points measured. **(B)** Western blotting analyses of *Rosa26*$^{+/CreER\text{-}T2}$*Ctip*$^{co/co}$ and *Rosa26*$^{+/CreER\text{-}T2}$*Ctip*$^{co/co}$*Ku70*$^{-/-}$ Abelson cells upon *Ctip* inactivation (days 1 and 3). **(C)** Representative cell cycle analyses of *Rosa26*$^{+/CreER\text{-}T2}$*Ctip*$^{co/co}$ and *Rosa26*$^{+/CreER\text{-}T2}$*Ctip*$^{co/co}$*Ku70*$^{-/-}$ Abelson cells after Cre activation. The boxes mark the sub-G1, G1, S (BrdU^{+}), and G2 populations. The data represent the average and SD of $n \geq 3$ biological repeats. **(D)** Representative cell viability analyses for *Rosa26*$^{+/CreER\text{-}T2}$*Ctip*$^{co/co}$ cells treated with ATR kinase inhibitor (ATRi) and/or 4OHT to active Cre recombination. The data represent the average and SD of $n \geq 3$ biological repeats. **(E)** Western blotting analyses of *Rosa26*$^{+/CreER\text{-}T2}$*Ctip*$^{co/co}$ treated with ATM (ATMi) or ATR (ATRi) kinase inhibitors.

Several mechanisms have been proposed to explain the impact of CtIP on CSR, including its ability to modulate activation-induced cytidine deaminase function, DNA end joining, CDK2 regulation or, less directly, cell proliferation (Lee-Theilen et al., 2011; Buis et al., 2012; Polato et al., 2014). CtIP-knockdown or CtIP-depleted cells have major proliferation defects, which could indirectly affect CSR. Indeed, sensitive CellTrace Violet (CTV) labeling (Fig. 4 C) suggest that even *Ctip*$^{T855A/T855A}$ B cells have a slight proliferation disadvantage. Yet, the CSR efficiency of *Ctip*$^{T855A/T855A}$ B is not significantly different from *Ctip*$^{+/+}$ B with the same doubling (Fig. 4 C). Together with the normal distribution of the CSR junctions and MH usage in the *Ctip*$^{T855A/T855A}$ B cells (Fig. 4, D and E), we conclude that the CSR defects in CtIP-deficient cells in large part reflect the inability of these cells to proliferate normally. In the case of *Ctip*$^{T855A/T855A}$ B cells, the switching frequency in cells with six or more divisions is slightly higher than that of *Ctip*$^{+/+}$ B cells (Fig. 4 C), suggesting the transient CSR delay in early time points might be compensated by extensive proliferation of successfully switched *Ctip*$^{T855A/T855A}$ B cells.

Finally, using the conditional allele and acute inactivation of CtIP in proliferating B cells, we show that while not essential for the initiation of DNA replication, CtIP processes spontaneous replication/recombination intermediates during S or G2 phase. While the exact nature of these intermediates remains elusive, previous studies suggest that CtIP can process protein–DNA adducts (Nakamura et al., 2010; Aparicio et al., 2016), DNA secondary structures (e.g., common fragile sites or palindromic sequences; Makharashvili et al., 2014; Wang et al., 2014), and DNA hairpins (Lengsfeld et al., 2007; Makharashvili et al., 2014; Wang et al., 2014; Chen et al., 2015). Deletion of the *BRCA2* tumor suppressor, specifically loss of its HR function, elicits a similar mode of cell lethality as *Ctip*$^{-/-}$ cells, marked by ATM hyperactivation, G2/M arrest, and formation of 53BP1 nuclear bodies (Feng and Jasin, 2017). As HR is also dependent on the DNA resection activity of CtIP (Sartori et al., 2007), similar replication/recombination intermediates may be responsible for the loss of cell viability in both *Brca2*- and *Ctip*-deleted cells. The normal response of

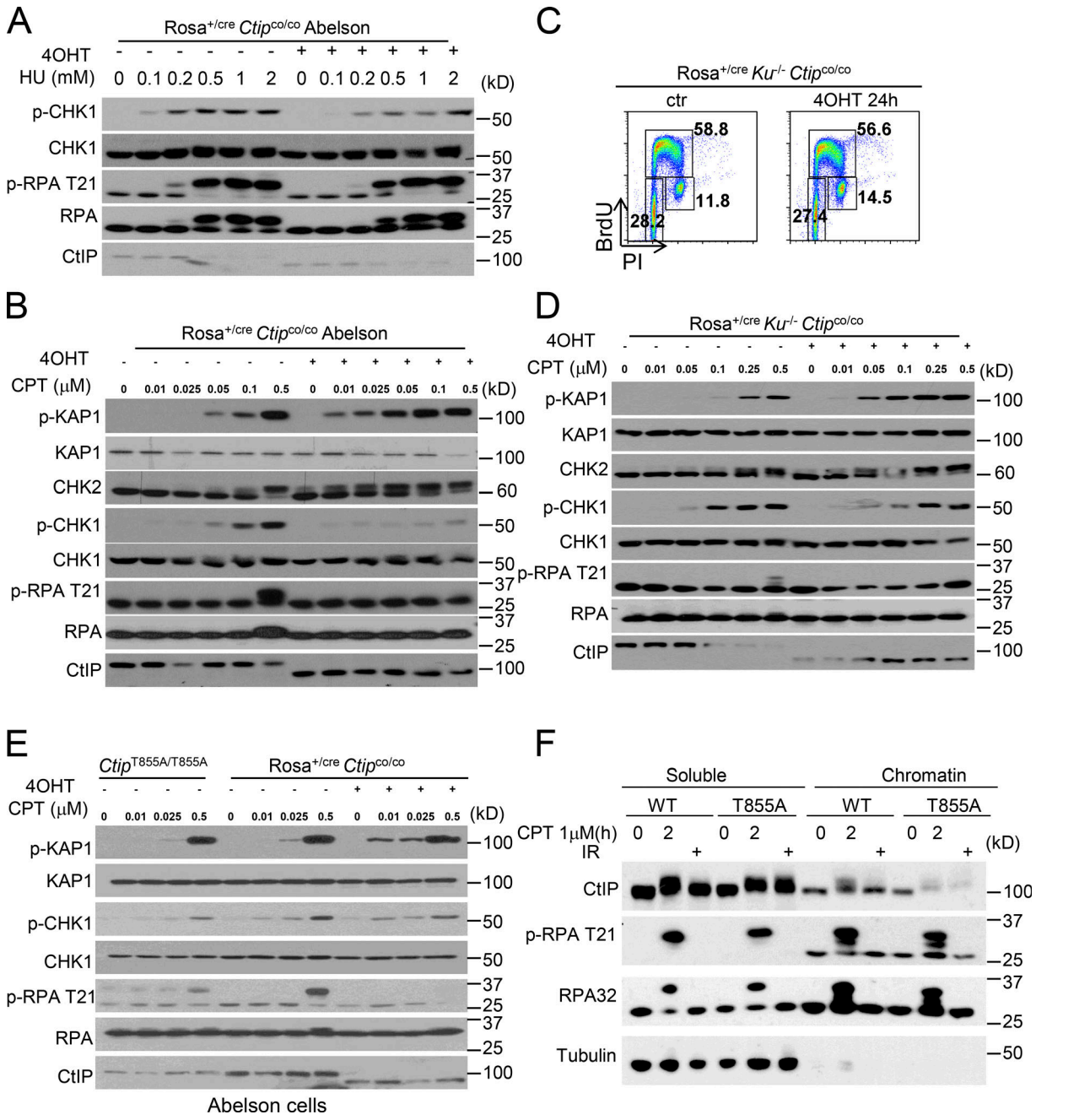

Figure 7. **DNA damage response of CtIP-deficient B cells. (A and B)** Western blotting analyses of (A) HU (0.1, 0.2, 0.5, and 1 mM, 1 h)– or (B) CPT (10, 25, 50, 100, and 500 nM)–induced DNA damage responses in *Rosa26*$^{+/CreER\text{-}T2}$*Ctip*$^{co/co}$ cells (with or without 4OHT for 24 h). **(C)** Cell cycle analyses of *Rosa26*$^{+/CreER\text{-}T2}$*Ctip*$^{co/co}$*Ku70*$^{-/-}$ cells with or without 4OHT for 24 h. The boxes mark the sub-G1, G1, S (BrdU^{+}), and G2 populations. **(D)** Western blotting analyses of CPT (10, 25, 50, 100, and 500 nM) induced DNA damage responses in *Rosa26*$^{+/CreER\text{-}T2}$*Ctip*$^{co/co}$*Ku70*$^{-/-}$ cells (with or without 4OHT for 24 h). **(E)** Western blotting analyses of CPT (10, 25, 50, 100, 500 nM)–induced DNA damage responses in *Ctip*$^{T855A/T855A}$ and control 4OHT-treated *Rosa26*$^{+/CreER\text{-}T2}$*Ctip*$^{co/co}$ cells (24 h). **(F)** Western blotting analyses of the chromatin and soluble fractionation assay of *Ctip*$^{+/+}$ (WT) and *Ctip*$^{T855A/T855A}$ v-abl cells after CPT (1 μM, 2 h) or IR (10 Gy, ∼15 min) treatment. The experiments were repeated three times, and one representative result is shown.

CtIP-deficient B cells to HU- or IR-induced breaks, but not CPT-induced breaks, further suggests that CtIP processes complex replication intermediates, including a potential hairpin structure, to support early B cell development and CSR in a CDK-dependent (i.e., CtIP-T847 phosphorylation) and ATR/ATM-independent (e.g., CtIP-T859 phosphorylation) manner.

Materials and methods

Mice

Ctip$^{+/co}$ (Bothmer et al., 2013), *CD21Cre* (Kraus et al., 2001), *Mb1Cre* (Hobeika et al., 2006), and *Rosa26*$^{+/CreER\text{-}T}$ (Guo et al., 2007) mice were previously characterized. Artemis-deficient mice (Rooney et al., 2002) were used as controls for B cell and thymocyte development. All animal work was conducted in a

specific pathogen–free facility, and all procedures were approved by the Institutional Animal Care and Use Committee at Columbia University Medical Center.

Generation of v-abl–transformed B cells and V(D)J recombination efficiency and junction analyses

Total bone marrow was isolated from 1-mo-old Eμ-Bcl2 transgenic mice (or embryonic day 14.5 fetal liver) and infected with a retrovirus encoding the v-abl kinase (Bredemeyer et al., 2006). Cells were maintained in DMEM (GIBCO) supplemented with 15% (vol/vol) FBS for 6–8 wk before the cells were infected with retrovirus encoding the V(D)J recombination substrates (pMX-INV; Bredemeyer et al., 2006). To perform the assay, v-abl–transformed B cells with stable integration pMX-INV were treated with STI571 (3 μM; Novartis Pharmaceuticals) and collected at 0, 2, or 4 d for FACS analyses of GFP expression and Southern blotting for rearrangement. Specifically, genomic DNA was digested with EcoRV or EcoRV+NcoI and probed with the hCD4 probe as detailed in the Fig. 2 legend (Liu et al., 2012). The hCD4 probe was PCR amplified with primers (5′-GTTCGG ATTGACTGCCAACT-3′ and 5′-GATGCCTAGCCCAATGAAAA-3′) from the pMX-INV plasmid. When indicated, the ATM inhibitor (Ku55933; Selleckchem) was added to a final concentration of 15 μM. The de novo CJs on the pMX-INV substrates were amplified with primers 5′-ACAACCACTACCTGAGCACC-3′ and 5′-TTGCATTCCTTTGGCGAGAG-3′ (~400-bp products), and the SJs were amplified via 5′-ACCAAGAACAACTGGACCGA-3′ and 5′-CGTAGGTCAGGGTGGTCAC-3′ (~550 bp). The precise SJs reconstitute an ApaL1 cutting site, which is used to determine fidelity.

The endogenous V(D)J recombination junctions were analyzed as previously described (Liu et al., 2017). DNA from purified splenic B cells were amplified via nesting PCR, first with JH_DQ52 (5′-TGATAGGCACCCAAGTACACTA -3′) and JH4 Int (5′-CCTCTCCAGTTTCGGCTGAATCC-3′) and then with the same JH_DQ52 primers and JH4E (5′-AGGCTCTGAGATCCCTAGACA G-3′). The ~536-bp amplicon corresponding to DQ52-JH4 junctions were isolated and cloned into pGEM-T (Promega) and sequenced. Vβ14-DJβ1 SJs were amplified from thymocyte DNA with Vβ14DJ1_SJ_F (5′-GGCAAGGGCAAAGCTAGGCTAGAT-3′) and Vβ14DJ1_SJ_R (5′-GCATGCCCAGCGTACCTCAATAG-3′). Vβ14DJβ1 CJs were amplified with Vβ14F (5′-AGAGTCGGTGGT GCAACTGAACCT-3′) and reverse P2 (5′-CCTGACTTCCACCCG AGGTTC-3′). Two amplicons corresponding to rearrangements involving Jβ1.1 (~550 bp) and Jβ1.2 (~370 bp), respectively, were isolated from each sample. For both SJ and CJ, the amplicons were gel purified and cloned into a pGM-T Fast Vector (VT207-02; Tiangen) and sequenced. The unique junctions were aligned with germline IgH or TCRβ14 sequences to identify the palindromic element and nontemplate nucleotide addition.

Terminal deoxynucleotidyl transferase (TdT)–assisted PCR assay

2 μg genomic DNA was treated with TdT (New England Biolabs) according to the manufacturer's protocol in the presence of 5 μM dATP, and the reaction was terminated by heating to 70°C for 15 min. 2% of the reaction was used for primary amplification (15 cycles) with primers IRES-REV5 (5′ REV5; 5′-CTCGACTAAACA CATGTAAAGCCTCGACTAAACACATGTAAAGC-3′) and T17- UNIV (5′-GTAAAACGACGGCCAGTCGACTTTTTTTTTTTTTTT-3′). 2% of the products of the primary amplification and serial 1:5 dilutions were used as templates for a second amplification step (17 cycles) using primers IRES-REV4 (5′-AGTGTAGAATTCCCCTTG TTGAATACGCTTG-3′) and UNIV (5′-AGAGCTGGATCCGTAAAA CGACGGCCAGT-3′). The secondary reaction products (~500 bp) were analyzed on 1% agarose gel, transferred onto a Zeta-Probe membrane (Bio-Rad), and hybridized with the ^{32}P-labeled hCD4 probe as described before. A PCR product (~700 bp) from the Rosa26a locus was amplified as control as described previously (Jiang et al., 2015).

Lymphocyte development and CSR

Lymphocytes of the thymus, bone marrow, spleen, and LN from 4–6-wk-old mice of the described genotypes were made into ~1 × 10^5 cells ml^{-1} single-cell suspensions, which were stained using fluorescence-conjugated antibodies before analyzed by flow cytometry. For the CSR assay, CD43$^-$ splenic B cells were purified using anti-murine CD43 magnetic beads (MACS; Miltenyi Biotech) and cultured at 0.5 × 10^6 cells ml^{-1} in RPMI medium supplemented with 15% FBS and 25 ng ml^{-1} of LPS plus 25 ng ml^{-1} of IL-4 (R&D). Cultured cells were maintained daily at a density of 0.5–1.0 × 10^6 cells ml^{-1}. Cells were collected 2–4 d after activation for flow cytometry with FITC-conjugated anti-IgG1 (BD PharMingen) and Cyc3-conjugated anti-murine B220 (eBioscience). Flow cytometry was performed on a FACSCalibur flow cytometer (BD Bioscience) and the data processed using FlowJo software package.

Construction of plasmids

pBMN-Flag-IRES-hCD2 plasmid was constructed as described before (Liu et al., 2012). An expression vector encoding Flag-tagged full-length WT human CTIP (Fl3-siCtIP/pCIN4) was subjected to site-directed mutagenesis to generate vectors expressing CtIP derivatives bearing the T847A, T847E, T859A, T859E, or E157K missense mutations, or the ΔPLDLS deletion mutation. A human CtIP expression plasmid containing the combined S231A/S664A/S745A missense mutation was a gift from Dr. Tanya Paull (The University of Texas at Austin, Austin, TX; Lengsfeld et al., 2007; Makharashvili et al., 2014; Wang et al., 2014; Chen et al., 2015). The pBMN-Flag-CTIP-IRES-hCD2 plasmid was used to transfect Phoenix cells and generate retrovirus. Infections were performed with ~3 × 10^6 cells in the presence of 12 μg/ml polybrene for 3 h with spin (~500 *g*) at room temperature.

Chromatin fractionation, western blot, and antibodies

Cells were lysed in radioimmunoprecipitation assay buffer (50 mM Tris-HCl, pH 8.0, 150 mM NaCl, 0.1% SDS, 0.5% sodium deoxycholate, 1% NP-40, and fresh proteinase inhibitor cocktail) following standard Western blotting protocols and blotted with antibodies specific for Flag (M2, 1:5,000, F3165; Sigma-Aldrich), CtIP (1:1,000; Yu and Baer, 2000), anti-pho-KAP1 (1:1,000, A300-767A; Bethyl Laboratories), anti-KAP1 (1:1,000, 4124S; Cell Signaling), anti-CHK1 (1:1,000, 2348S; Cell

Signaling), anti-pho-CHK1(S345) (1:1,000, 2348S; Cell Signaling), anti-RPA32 (1:10,000, A300-244A; Bethyl Laboratories), and anti-pho-RPA(T21) (1:10,000, ab19109394; Abcam). HRP-conjugated anti-rabbit and mouse secondary antibodies (GE Healthcare) were used, and an ECL Western blotting detection system (GE Healthcare) was used for detection.

For chromatin fractionation experiments, the cells were collected and washed with PBS once and then resuspended with 0.05% NP40 lysis buffer (50 mM Tris-HCl, pH 7.5, and 150 mM NaCl, with protease and phosphatase inhibitors) and incubated on ice for 30 min. After slow centrifugation (500 *g*, 5 min), the supernatant was collected into a new tube for a 15-min top-speed centrifugation. The supernatant from the high-speed spin was saved as "soluble fraction." The pellet from the first slow-centrifugation step was washed once with 0.1% NP-40 lysis buffer, without fully disturbing the pellet. After another slow centrifugation, the supernatant was discarded and the pellet was resuspended with 0.5% NP-40 lysis buffer with 125 U/ml Benzonase (Novegan) and incubated on ice for 1 h. The reaction was stopped by adding EDTA to a 5 µM final concentration, followed by a 15-min top-speed centrifugation, and the supernatant was collected as chromatin fraction. For each sample, the volume of the 0.5% NP-40 lysis buffer used for chromatin fraction was one tenth of the 0.05% NP-40 lysis buffer for the soluble fraction, and the two fractions were loaded the same volume for Western blot analysis.

High-throughput genome-wide translocation sequencing (HTGTS)

HTGTS was performed as previously described (Dong et al., 2015; Hu et al., 2016; Panchakshari et al., 2018). Genomic DNA was collected from activated B cells after 4 d, sonicated (Diagenode Bioruptor), and amplified with Sµ-specific biotin primer (5′/5BiosG/CAGACCTGGGAATGTATGGT-3′) and nested (5′-CACACAAAGACTCTGGACCTC-3′) primers. AflII is used to remove the germline sequence. All mice analyzed here have the IgH locus in the C57/BL6 background; thus, the standard mm9 genome was used for alignment. Sequences were analyzed as detailed before (Dong et al., 2015; Hu et al., 2016). The best-path searching algorithm (related to YAHA, a fast and flexible hash-based aligner; Faust and Hall, 2012) was used to identify optimal sequence alignments from Bowtie2-reported top alignments (alignment score >50). The reads are then filtered to exclude mispriming events, germline (unmodified) sequence, sequential joints, and duplicated reads. A "duplicate read" is defined by bait and prey alignment coordinates within 2 nt of another read's bait and prey alignments. To plot all the S-region junctions, including those in the repeats but unequivocally mapped to an individual switch region, we combined the ones filtered by a mappability filter but unequivocally mapped to S regions with "good" reads passing both the mappability (both de-duplicated) filters (please see Dong et al., 2015 for simulation and details on plotting). MHs are defined as regions of 100% homology between the bait and prey–break site. Insertions are defined as regions containing nucleotides that map to neither the bait nor the prey–break site. Blunt junctions are considered to have no MHs or insertions. The HTGTS data reported in this paper have been deposited in the Gene Expression Omnibus database with the accession no. GSE129850.

Online supplemental material

Fig. S1 shows significant cell cycle defects and normal end joining in *Ctip*-deficient B cells. Fig. S2 shows the intrinsic nuclease activity of CtIP is not required cellular viability. Fig. S3 shows that CtIP T859 (T855 in mouse) phosphorylation is not required for normal lymphocyte development. Fig. S4 shows that CtIP is not essential for the initiation of DNA replication in B cells. Table S1 shows lymphocyte number and frequency and V(D)J recombination junctions in CtIP-deficient mice.

Acknowledgments

We thank Drs. Lorraine Symington and Max Gottesman for helpful discussions.

This work was supported in part by National Institutes of Health/National Cancer Institute grants 5R01CA158073, 5R01CA184187, and 1P01CA174653 to S. Zha and National Institutes of Health grant 1P01CA174653 to R. Baer and J. Gautier. This research was funded in part through National Institutes of Health/National Cancer Institute Cancer Center Support Grant P30CA013696 to Herbert Irving Comprehensive Cancer Center of Columbia University. The sequencing and analyses of the TCRβ junctions were supported by the Discipline Construction Funding of Shenzhen (2016) to X. Liu. S. Zha is a recipient of the Leukemia and Lymphoma Society Scholar Award, and X. Liu was a Leukemia and Lymphoma Society Fellow.

The authors declare no competing financial interests.

Author contributions: X. Liu, X.S. Wang, S. Zha, and R. Baer designed experiments. S. Zha and R. Baer wrote the paper. S. Zha analyzed the Mb1CreCtip conditional mouse models. X.S. Wang, B.J. Lee, V.M. Estes, and S. Zha analyzed CD21Cre Ctip conditional mouse models. X. Liu generated and analyzed the *Rosa26*$^{+/CreER\text{-}T2}$*Ctip*$^{co/co}$ cells and performed the genetic complementation experiments. S. Zha, R. Baer, and J. Gautier conceived the experiments to test the role of T859 phosphorylation in CtIP function. R.J. Baer and F.K. Wu-Baer generated the mice carrying the *Ctip*^{T855A} allele. X. Liu, X.S. Wang, and X. Lin analyzed lymphocyte development in the *Ctip*$^{T855A/T855A}$ mice. X. Liu and X.S. Wang generated and analyzed the *Ctip*$^{T855A/T855A}$ v-abl B cells.

Submitted: 16 June 2018
Revised: 10 September 2018
Accepted: 24 April 2019

References

Andres, S.N., C.D. Appel, J.W. Westmoreland, J.S. Williams, Y. Nguyen, P.D. Robertson, M.A. Resnick, and R.S. Williams. 2015. Tetrameric Ctp1 coordinates DNA binding and DNA bridging in DNA double-strand-break repair. *Nat. Struct. Mol. Biol.* 22:158–166. https://doi.org/10.1038/nsmb.2945

Aparicio, T., R. Baer, M. Gottesman, and J. Gautier. 2016. MRN, CtIP, and BRCA1 mediate repair of topoisomerase II-DNA adducts. *J. Cell Biol.* 212: 399–408. https://doi.org/10.1083/jcb.201504005

Barton, O., S.C. Naumann, R. Diemer-Biehs, J. Künzel, M. Steinlage, S. Conrad, N. Makharashvili, J. Wang, L. Feng, B.S. Lopez, et al. 2014. Polo-like kinase 3 regulates CtIP during DNA double-strand break repair in G1. *J. Cell Biol.* 206:877–894. https://doi.org/10.1083/jcb.201401146

Beamish, H., K.K. Khanna, and M.F. Lavin. 1994. Ionizing radiation and cell cycle progression in ataxia telangiectasia. *Radiat. Res.* 138(1, Suppl): S130–S133. https://doi.org/10.2307/3578780

Borghesani, P.R., F.W. Alt, A. Bottaro, L. Davidson, S. Aksoy, G.A. Rathbun, T.M. Roberts, W. Swat, R.A. Segal, and Y. Gu. 2000. Abnormal development of Purkinje cells and lymphocytes in Atm mutant mice. *Proc. Natl. Acad. Sci. USA.* 97:3336–3341. https://doi.org/10.1073/pnas.97.7.3336

Bothmer, A., P.C. Rommel, A. Gazumyan, F. Polato, C.R. Reczek, M.F. Muellenbeck, S. Schaetzlein, W. Edelmann, P.L. Chen, R.M. Brosh Jr., et al. 2013. Mechanism of DNA resection during intrachromosomal recombination and immunoglobulin class switching. *J. Exp. Med.* 210:115–123.

Bredemeyer, A.L., G.G. Sharma, C.Y. Huang, B.A. Helmink, L.M. Walker, K.C. Khor, B. Nuskey, K.E. Sullivan, T.K. Pandita, C.H. Bassing, and B.P. Sleckman. 2006. ATM stabilizes DNA double-strand-break complexes during V(D)J recombination. *Nature.* 442:466–470. https://doi.org/10.1038/nature04866

Buis, J., T. Stoneham, E. Spehalski, and D.O. Ferguson. 2012. Mre11 regulates CtIP-dependent double-strand break repair by interaction with CDK2. *Nat. Struct. Mol. Biol.* 19:246–252. https://doi.org/10.1038/nsmb.2212

Cannavo, E., and P. Cejka. 2014. Sae2 promotes dsDNA endonuclease activity within Mre11-Rad50-Xrs2 to resect DNA breaks. *Nature.* 514:122–125. https://doi.org/10.1038/nature13771

Chen, H., R.A. Donnianni, N. Handa, S.K. Deng, J. Oh, L.A. Timashev, S.C. Kowalczykowski, and L.S. Symington. 2015. Sae2 promotes DNA damage resistance by removing the Mre11-Rad50-Xrs2 complex from DNA and attenuating Rad53 signaling. *Proc. Natl. Acad. Sci. USA.* 112: E1880–E1887. https://doi.org/10.1073/pnas.1503331112

Chen, L., C.J. Nievera, A.Y. Lee, and X. Wu. 2008. Cell cycle-dependent complex formation of BRCA1.CtIP.MRN is important for DNA double-strand break repair. *J. Biol. Chem.* 283:7713–7720. https://doi.org/10.1074/jbc.M710245200

Chen, P.L., F. Liu, S. Cai, X. Lin, A. Li, Y. Chen, B. Gu, E.Y. Lee, and W.H. Lee. 2005. Inactivation of CtIP leads to early embryonic lethality mediated by G1 restraint and to tumorigenesis by haploid insufficiency. *Mol. Cell. Biol.* 25:3535–3542. https://doi.org/10.1128/MCB.25.9.3535-3542.2005

Davies, O.R., J.V. Forment, M. Sun, R. Belotserkovskaya, J. Coates, Y. Galanty, M. Demir, C.R. Morton, N.J. Rzechorzek, S.P. Jackson, and L. Pellegrini. 2015. CtIP tetramer assembly is required for DNA-end resection and repair. *Nat. Struct. Mol. Biol.* 22:150–157. https://doi.org/10.1038/nsmb.2937

Deshpande, R.A., J.H. Lee, S. Arora, and T.T. Paull. 2016. Nbs1 Converts the Human Mre11/Rad50 Nuclease Complex into an Endo/Exonuclease Machine Specific for Protein-DNA Adducts. *Mol. Cell.* 64:593–606. https://doi.org/10.1016/j.molcel.2016.10.010

Difilippantonio, S., E. Gapud, N. Wong, C.Y. Huang, G. Mahowald, H.T. Chen, M.J. Kruhlak, E. Callen, F. Livak, M.C. Nussenzweig, et al. 2008. 53BP1 facilitates long-range DNA end-joining during V(D)J recombination. *Nature.* 456:529–533. https://doi.org/10.1038/nature07476

Dong, J., R.A. Panchakshari, T. Zhang, Y. Zhang, J. Hu, S.A. Volpi, R.M. Meyers, Y.J. Ho, Z. Du, D.F. Robbiani, et al. 2015. Orientation-specific joining of AID-initiated DNA breaks promotes antibody class switching. *Nature.* 525:134–139. https://doi.org/10.1038/nature14970

Dubin, M.J., P.H. Stokes, E.Y. Sum, R.S. Williams, V.A. Valova, P.J. Robinson, G.J. Lindeman, J.N. Glover, J.E. Visvader, and J.M. Matthews. 2004. Dimerization of CtIP, a BRCA1- and CtBP-interacting protein, is mediated by an N-terminal coiled-coil motif. *J. Biol. Chem.* 279:26932–26938. https://doi.org/10.1074/jbc.M313974200

Faust, G.G., and I.M. Hall. 2012. YAHA: fast and flexible long-read alignment with optimal breakpoint detection. *Bioinformatics.* 28:2417–2424. https://doi.org/10.1093/bioinformatics/bts456

Feng, W., and M. Jasin. 2017. BRCA2 suppresses replication stress-induced mitotic and G1 abnormalities through homologous recombination. *Nat. Commun.* 8:525. https://doi.org/10.1038/s41467-017-00634-0

Forment, J.V., S.P. Jackson, and L. Pellegrini. 2015. When two is not enough: a CtIP tetramer is required for DNA repair by Homologous Recombination. *Nucleus.* 6:344–348. https://doi.org/10.1080/19491034.2015.1086050

Franco, S., F.W. Alt, and J.P. Manis. 2006. Pathways that suppress programmed DNA breaks from progressing to chromosomal breaks and translocations. *DNA Repair (Amst.).* 5:1030–1041. https://doi.org/10.1016/j.dnarep.2006.05.024

Fusco, C., A. Reymond, and A.S. Zervos. 1998. Molecular cloning and characterization of a novel retinoblastoma-binding protein. *Genomics.* 51: 351–358. https://doi.org/10.1006/geno.1998.5368

Guo, K., J.E. McMinn, T. Ludwig, Y.H. Yu, G. Yang, L. Chen, D. Loh, C. Li, S. Chua Jr., and Y. Zhang. 2007. Disruption of peripheral leptin signaling in mice results in hyperleptinemia without associated metabolic abnormalities. *Endocrinology.* 148:3987–3997. https://doi.org/10.1210/en.2007-0261

Helmink, B.A., A.T. Tubbs, Y. Dorsett, J.J. Bednarski, L.M. Walker, Z. Feng, G.G. Sharma, P.J. McKinnon, J. Zhang, C.H. Bassing, and B.P. Sleckman. 2011. H2AX prevents CtIP-mediated DNA end resection and aberrant repair in G1-phase lymphocytes. *Nature.* 469:245–249. https://doi.org/10.1038/nature09585

Hobeika, E., S. Thiemann, B. Storch, H. Jumaa, P.J. Nielsen, R. Pelanda, and M. Reth. 2006. Testing gene function early in the B cell lineage in mb1-cre mice. *Proc. Natl. Acad. Sci. USA.* 103:13789–13794. https://doi.org/10.1073/pnas.0605944103

Hu, J., R.M. Meyers, J. Dong, R.A. Panchakshari, F.W. Alt, and R.L. Frock. 2016. Detecting DNA double-stranded breaks in mammalian genomes by linear amplification-mediated high-throughput genome-wide translocation sequencing. *Nat. Protoc.* 11:853–871. https://doi.org/10.1038/nprot.2016.043

Huertas, P., F. Cortés-Ledesma, A.A. Sartori, A. Aguilera, and S.P. Jackson. 2008. CDK targets Sae2 to control DNA-end resection and homologous recombination. *Nature.* 455:689–692. https://doi.org/10.1038/nature07215

Jiang, W., J.L. Crowe, X. Liu, S. Nakajima, Y. Wang, C. Li, B.J. Lee, R.L. Dubois, C. Liu, X. Yu, et al. 2015. Differential phosphorylation of DNA-PKcs regulates the interplay between end-processing and end-ligation during nonhomologous end-joining. *Mol. Cell.* 58:172–185. https://doi.org/10.1016/j.molcel.2015.02.024

Jonkers, J., R. Meuwissen, H. van der Gulden, H. Peterse, M. van der Valk, and A. Berns. 2001. Synergistic tumor suppressor activity of BRCA2 and p53 in a conditional mouse model for breast cancer. *Nat. Genet.* 29:418–425. https://doi.org/10.1038/ng747

Kraus, M., L.I. Pao, A. Reichlin, Y. Hu, B. Canono, J.C. Cambier, M.C. Nussenzweig, and K. Rajewsky. 2001. Interference with immunoglobulin (Ig)alpha immunoreceptor tyrosine-based activation motif (ITAM) phosphorylation modulates or blocks B cell development, depending on the availability of an Igbeta cytoplasmic tail. *J. Exp. Med.* 194:455–469. https://doi.org/10.1084/jem.194.4.455

Kraus, M., M.B. Alimzhanov, N. Rajewsky, and K. Rajewsky. 2004. Survival of resting mature B lymphocytes depends on BCR signaling via the Ig-alpha/beta heterodimer. *Cell.* 117:787–800. https://doi.org/10.1016/j.cell.2004.05.014

Lee-Theilen, M., A.J. Matthews, D. Kelly, S. Zheng, and J. Chaudhuri. 2011. CtIP promotes microhomology-mediated alternative end joining during class-switch recombination. *Nat. Struct. Mol. Biol.* 18:75–79. https://doi.org/10.1038/nsmb.1942

Lengsfeld, B.M., A.J. Rattray, V. Bhaskara, R. Ghirlando, and T.T. Paull. 2007. Sae2 is an endonuclease that processes hairpin DNA cooperatively with the Mre11/Rad50/Xrs2 complex. *Mol. Cell.* 28:638–651. https://doi.org/10.1016/j.molcel.2007.11.001

Liu, F., and W.H. Lee. 2006. CtIP activates its own and cyclin D1 promoters via the E2F/RB pathway during G1/S progression. *Mol. Cell. Biol.* 26: 3124–3134. https://doi.org/10.1128/MCB.26.8.3124-3134.2006

Liu, X., W. Jiang, R.L. Dubois, K. Yamamoto, Z. Wolner, and S. Zha. 2012. Overlapping functions between XLF repair protein and 53BP1 DNA damage response factor in end joining and lymphocyte development. *Proc. Natl. Acad. Sci. USA.* 109:3903–3908. https://doi.org/10.1073/pnas.1120160109

Liu, X., Z. Shao, W. Jiang, B.J. Lee, and S. Zha. 2017. PAXX promotes KU accumulation at DNA breaks and is essential for end-joining in XLF-deficient mice. *Nat. Commun.* 8:13816. https://doi.org/10.1038/ncomms13816

Lukas, C., V. Savic, S. Bekker-Jensen, C. Doil, B. Neumann, R.S. Pedersen, M. Grøfte, K.L. Chan, I.D. Hickson, J. Bartek, and J. Lukas. 2011. 53BP1 nuclear bodies form around DNA lesions generated by mitotic transmission of chromosomes under replication stress. *Nat. Cell Biol.* 13: 243–253. https://doi.org/10.1038/ncb2201

Ma, Y., U. Pannicke, K. Schwarz, and M.R. Lieber. 2002. Hairpin opening and overhang processing by an Artemis/DNA-dependent protein kinase complex in nonhomologous end joining and V(D)J recombination. *Cell.* 108:781–794. https://doi.org/10.1016/S0092-8674(02)00671-2

Makharashvili, N., A.T. Tubbs, S.H. Yang, H. Wang, O. Barton, Y. Zhou, R.A. Deshpande, J.H. Lee, M. Lobrich, B.P. Sleckman, et al. 2014. Catalytic

and noncatalytic roles of the CtIP endonuclease in double-strand break end resection. *Mol. Cell.* 54:1022–1033. https://doi.org/10.1016/j.molcel.2014.04.011

McVey, M., and S.E. Lee. 2008. MMEJ repair of double-strand breaks (director's cut): deleted sequences and alternative endings. *Trends Genet.* 24:529–538. https://doi.org/10.1016/j.tig.2008.08.007

Mimitou, E.P., and L.S. Symington. 2008. Sae2, Exo1 and Sgs1 collaborate in DNA double-strand break processing. *Nature.* 455:770–774. https://doi.org/10.1038/nature07312

Mimitou, E.P., and L.S. Symington. 2010. Ku prevents Exo1 and Sgs1-dependent resection of DNA ends in the absence of a functional MRX complex or Sae2. *EMBO J.* 29:3358–3369. https://doi.org/10.1038/emboj.2010.193

Moshous, D., I. Callebaut, R. de Chasseval, B. Corneo, M. Cavazzana-Calvo, F. Le Deist, I. Tezcan, O. Sanal, Y. Bertrand, N. Philippe, et al. 2001. Artemis, a novel DNA double-strand break repair/V(D)J recombination protein, is mutated in human severe combined immune deficiency. *Cell.* 105:177–186. https://doi.org/10.1016/S0092-8674(01)00309-9

Nakamura, K., T. Kogame, H. Oshiumi, A. Shinohara, Y. Sumitomo, K. Agama, Y. Pommier, K.M. Tsutsui, K. Tsutsui, E. Hartsuiker, et al. 2010. Collaborative action of Brca1 and CtIP in elimination of covalent modifications from double-strand breaks to facilitate subsequent break repair. *PLoS Genet.* 6:e1000828. https://doi.org/10.1371/journal.pgen.1000828

Oksenych, V., F.W. Alt, V. Kumar, B. Schwer, D.R. Wesemann, E. Hansen, H. Patel, A. Su, and C. Guo. 2012. Functional redundancy between repair factor XLF and damage response mediator 53BP1 in V(D)J recombination and DNA repair. *Proc. Natl. Acad. Sci. USA.* 109:2455–2460. https://doi.org/10.1073/pnas.1121458109

Panchakshari, R.A., X. Zhang, V. Kumar, Z. Du, P.C. Wei, J. Kao, J. Dong, and F.W. Alt. 2018. DNA double-strand break response factors influence end-joining features of IgH class switch and general translocation junctions. *Proc. Natl. Acad. Sci. USA.* 115:762–767. https://doi.org/10.1073/pnas.1719988115

Peterson, S.E., Y. Li, F. Wu-Baer, B.T. Chait, R. Baer, H. Yan, M.E. Gottesman, and J. Gautier. 2013. Activation of DSB Processing Requires Phosphorylation of CtIP by ATR. *Mol. Cell.* 49:657–667.

Polato, F., E. Callen, N. Wong, R. Faryabi, S. Bunting, H.T. Chen, M. Kozak, M.J. Kruhlak, C.R. Reczek, W.H. Lee, et al. 2014. CtIP-mediated resection is essential for viability and can operate independently of BRCA1. *J. Exp. Med.* 211:1027–1036. https://doi.org/10.1084/jem.20131939

Reczek, C.R., M. Szabolcs, J.M. Stark, T. Ludwig, and R. Baer. 2013. The interaction between CtIP and BRCA1 is not essential for resection-mediated DNA repair or tumor suppression. *J. Cell Biol.* 201:693–707. https://doi.org/10.1083/jcb.201302145

Rickert, R.C., J. Roes, and K. Rajewsky. 1997. B lymphocyte-specific, Cre-mediated mutagenesis in mice. *Nucleic Acids Res.* 25:1317–1318. https://doi.org/10.1093/nar/25.6.1317

Rooney, S., J. Sekiguchi, C. Zhu, H.L. Cheng, J. Manis, S. Whitlow, J. DeVido, D. Foy, J. Chaudhuri, D. Lombard, and F.W. Alt. 2002. Leaky Scid phenotype associated with defective V(D)J coding end processing in Artemis-deficient mice. *Mol. Cell.* 10:1379–1390. https://doi.org/10.1016/S1097-2765(02)00755-4

Sartori, A.A., C. Lukas, J. Coates, M. Mistrik, S. Fu, J. Bartek, R. Baer, J. Lukas, and S.P. Jackson. 2007. Human CtIP promotes DNA end resection. *Nature.* 450:509–514. https://doi.org/10.1038/nature06337

Schaeper, U., T. Subramanian, L. Lim, J.M. Boyd, and G. Chinnadurai. 1998. Interaction between a cellular protein that binds to the C-terminal region of adenovirus E1A (CtBP) and a novel cellular protein is disrupted by E1A through a conserved PLDLS motif. *J. Biol. Chem.* 273:8549–8552. https://doi.org/10.1074/jbc.273.15.8549

Symington, L.S., and J. Gautier. 2011. Double-strand break end resection and repair pathway choice. *Annu. Rev. Genet.* 45:247–271. https://doi.org/10.1146/annurev-genet-110410-132435

Unnikrishnan, I., A. Radfar, J. Jenab-Wolcott, and N. Rosenberg. 1999. p53 mediates apoptotic crisis in primary Abelson virus-transformed pre-B cells. *Mol. Cell. Biol.* 19:4825–4831. https://doi.org/10.1128/MCB.19.7.4825

Wang, H., Z. Shao, L.Z. Shi, P.Y. Hwang, L.N. Truong, M.W. Berns, D.J. Chen, and X. Wu. 2012. CtIP protein dimerization is critical for its recruitment to chromosomal DNA double-stranded breaks. *J. Biol. Chem.* 287:21471–21480. https://doi.org/10.1074/jbc.M112.355354

Wang, H., L.Z. Shi, C.C. Wong, X. Han, P.Y. Hwang, L.N. Truong, Q. Zhu, Z. Shao, D.J. Chen, M.W. Berns, et al. 2013. The interaction of CtIP and Nbs1 connects CDK and ATM to regulate HR-mediated double-strand break repair. *PLoS Genet.* 9:e1003277. https://doi.org/10.1371/journal.pgen.1003277

Wang, H., Y. Li, L.N. Truong, L.Z. Shi, P.Y. Hwang, J. He, J. Do, M.J. Cho, H. Li, A. Negrete, et al. 2014. CtIP maintains stability at common fragile sites and inverted repeats by end resection-independent endonuclease activity. *Mol. Cell.* 54:1012–1021. https://doi.org/10.1016/j.molcel.2014.04.012

Wong, A.K., P.A. Ormonde, R. Pero, Y. Chen, L. Lian, G. Salada, S. Berry, Q. Lawrence, P. Dayananth, P. Ha, et al. 1998. Characterization of a carboxy-terminal BRCA1 interacting protein. *Oncogene.* 17:2279–2285. https://doi.org/10.1038/sj.onc.1202150

Xu, B., S.T. Kim, D.S. Lim, and M.B. Kastan. 2002. Two molecularly distinct G(2)/M checkpoints are induced by ionizing irradiation. *Mol. Cell. Biol.* 22:1049–1059. https://doi.org/10.1128/MCB.22.4.1049-1059.2002

Yu, X., and R. Baer. 2000. Nuclear localization and cell cycle-specific expression of CtIP, a protein that associates with the BRCA1 tumor suppressor. *J. Biol. Chem.* 275:18541–18549. https://doi.org/10.1074/jbc.M909494199

Yu, X., L.C. Wu, A.M. Bowcock, A. Aronheim, and R. Baer. 1998. The C-terminal (BRCT) domains of BRCA1 interact in vivo with CtIP, a protein implicated in the CtBP pathway of transcriptional repression. *J. Biol. Chem.* 273:25388–25392. https://doi.org/10.1074/jbc.273.39.25388

Zha, S., C. Guo, C. Boboila, V. Oksenych, H.L. Cheng, Y. Zhang, D.R. Wesemann, G. Yuen, H. Patel, P.H. Goff, et al. 2011a. ATM damage response and XLF repair factor are functionally redundant in joining DNA breaks. *Nature.* 469:250–254. https://doi.org/10.1038/nature09604

Zha, S., W. Jiang, Y. Fujiwara, H. Patel, P.H. Goff, J.W. Brush, R.L. Dubois, and F.W. Alt. 2011b. Ataxia telangiectasia-mutated protein and DNA-dependent protein kinase have complementary V(D)J recombination functions. *Proc. Natl. Acad. Sci. USA.* 108:2028–2033. https://doi.org/10.1073/pnas.1019293108

Zhang, Y., and M. Jasin. 2011. An essential role for CtIP in chromosomal translocation formation through an alternative end-joining pathway. *Nat. Struct. Mol. Biol.* 18:80–84. https://doi.org/10.1038/nsmb.1940

Zhang, Y.W., D.M. Otterness, G.G. Chiang, W. Xie, Y.C. Liu, F. Mercurio, and R.T. Abraham. 2005. Genotoxic stress targets human Chk1 for degradation by the ubiquitin-proteasome pathway. *Mol. Cell.* 19:607–618. https://doi.org/10.1016/j.molcel.2005.07.019

Zhang, Y.W., J. Brognard, C. Coughlin, Z. You, M. Dolled-Filhart, A. Aslanian, G. Manning, R.T. Abraham, and T. Hunter. 2009. The F box protein Fbx6 regulates Chk1 stability and cellular sensitivity to replication stress. *Mol. Cell.* 35:442–453. https://doi.org/10.1016/j.molcel.2009.06.030